Predicting Critical Transitions in ENSO Models. Part I: Methodology and Simple Models with Memory

DMITRY MUKHIN, EVGENY LOSKUTOV, ANNA MUKHINA, AND ALEXANDER FEIGIN

Institute of Applied Physics of Russian Academy of Sciences, and Lobachevsky State University of Nizhni Novgorod, Nizhny Novgorod, Russia

ILIA ZALIAPIN

Department of Mathematics and Statistics, University of Nevada, Reno, Reno, Nevada

MICHAEL GHIL

Geosciences Department, and Laboratoire de Météorologie Dynamique, CNRS and IPSL, École Normale Supérieure, Paris, France, and Department of Atmospheric and Oceanic Sciences, and Institute of Geophysics and Planetary Physics, University of California, Los Angeles, Los Angeles, California

(Manuscript received 28 March 2014, in final form 9 October 2014)

ABSTRACT

A new empirical approach is proposed for predicting critical transitions in the climate system based on a time series alone. This approach relies on nonlinear stochastic modeling of the system's time-dependent evolution operator by the analysis of observed behavior. Empirical models that take the form of a discrete random dynamical system are constructed using artificial neural networks; these models include state-dependent stochastic components. To demonstrate the usefulness of such models in predicting critical climate transitions, they are applied here to time series generated by a number of delay-differential equation (DDE) models of sea surface temperature anomalies. These DDE models take into account the main conceptual elements responsible for the El Niño–Southern Oscillation phenomenon. The DDE models used here have been modified to include slow trends in the control parameters in such a way that critical transitions occur beyond the learning interval in the time series. Numerical results suggest that the empirical models proposed herein are able to forecast sequences of critical transitions that manifest themselves in future abrupt changes of the climate system's statistics.

1. Introduction and motivation

Critical transitions are defined as abrupt changes in the statistical characteristics of a system's dynamics. Such changes are a well-known property of complex systems that include dynamic variables with distinct temporal scales (see, e.g., Scheffer 2009). Numerous examples of such systems are known in the physical, biological, and socioeconomic sciences. In particular, a system can exhibit critical transitions that modify a particular statistic on different time scales. For instance, in climate studies, the research can focus on transitions on multimillennial scales [e.g., the mid-Pleistocene transition in both amplitude and dominant periodicity of glacial cycles (Ghil 1994; Huybers 2009)] as well as on events with interannual time scales, exemplified by the 1976/77 transition in the dynamics of El Niño–Southern Oscillation (ENSO) and the Pacific decadal oscillation (Trenberth and Hurrel 1994; Chao et al. 2000).

Clearly, the physical principles that underly events on different time scales can also be very different. Such differences justify using simple conceptual models that describe only a few mechanisms of interest, as opposed to using more complex general circulation models, also called global climate models (GCMs). The latter describe a very large number of mechanisms, but tend to be "tuned" to current parameter values, which interferes with simulating climates that are very different from the one used for the tuning (Ghil and Robertson 2000; Ghil 2001).

Corresponding author address: Dmitry Mukhin, Institute of Applied Physics of Russian Academy of Sciences, 46 Ulyanova St., Nizhny Novgorod 603950, Russia.
E-mail: mukhin@appl.sci-nnov.ru

DOI: 10.1175/JCLI-D-14-00239.1

Forecasting critical transitions in real systems remains a difficult problem, even if the principal mechanisms of the dynamics are well captured by a conceptual model. The hopes for successfully forecasting a critical transition—namely, both its type and the instant of its onset—in a complex system can be based on assuming that the system's dynamics is described by a given, albeit unknown, evolution operator. The changes in the dynamical properties of such an operator govern the evolution of the observed system's statistics, while critical transitions correspond to bifurcations in the statistics, as described by the system's invariant measure (Eckmann and Ruelle 1985; Ghil et al. 2008a; Chekroun et al. 2011b).

GCMs that are based on first principles and provide a very detailed description of the observed phenomena are not well suited for the analysis of such bifurcations, or for the prediction of such events, mainly because of their high dimensionality: currently GCMs operate with an order of 10^6–10^7 discrete variables. These shortcomings have motivated researchers to develop coarser models of reduced complexity. Within the climate community, D. Kondrashov, S. Kravtsov, and coworkers have thus developed the empirical model reduction (EMR) approach, based on the reconstruction of a system of coupled nonlinear stochastic differential equations with colored noise from a model-simulated or observed time series (Kondrashov et al. 2005; Kravtsov et al. 2005, 2009). EMR models have been shown to be very skillful in simulating various statistical properties of the systems they have been used to study but have not been specifically applied to the problem of predicting critical transitions in the presence of slow changes in the system under investigation.

In a more general context, I.G. Kevrekidis and collaborators have developed an equation-free approach to the computation of bifurcations (Theodoropoulos et al. 2000; Runborg et al. 2002). This approach, however, has not been applied to the prediction of critical transitions, a prediction that might be called, following Timmermann and Jin (2006), a prediction of the third kind, as opposed to that involved in numerical weather forecasting or in seasonal prediction. In the first and most common one, we deal with an initial-value problem and the details of the solution are important, while in the second one, boundary data, such as sea surface temperatures (SSTs), also play an important role; furthermore, in the latter, one can only hope to predict certain coarse features of the solution, such as means and variances. In the predictability of critical transitions, one is interested in dramatic changes in the overall statistics of the solutions, and it is parameter values that play a decisive role.

In the present study, we propose an empirical modeling approach aimed at extracting crucial information about the evolution operator from an observed time series and applying it to the above prediction problem. The distinction between this approach and both detailed GCMs and simpler conceptual models consists in the absence of any a priori assumptions about the comparative role of various governing mechanisms and, therefore, about the structure of the model equations. Forecasting the system's behavior, including its critical transitions, is hence independent of various approximations connected to more detailed modeling approaches. The proposed reconstruction of the evolution operator from a time series only models the interactions reflected in the examined dataset and, hence, focuses on the processes that define the essential system dynamics on the analyzed time interval.

As usual in such empirical approaches, one has to assume that the interaction laws among the system's components that prevailed during the learning period can be extrapolated into the future. This assumption seems to hold for a fairly large class of systems, and it turns out to be the case for the models examined in this paper and its companion (Mukhin et al. 2015, hereinafter Part II). The persistence of the dynamical laws, and hence of the generated statistics, explains the predictive power of the empirical models proposed herein; for details, see Molkov et al. (2011, 2012). Below, we apply the general approach of Molkov et al. (2012) to model the atmosphere–ocean system in the equatorial Pacific Ocean that gives rise to the ENSO phenomenon, and thus predict its critical transitions.

Kondrashov et al. (2005) and Kravtsov et al. (2009) demonstrated the effectiveness of nonlinear, noise-driven EMR models—based solely on the observed time series of SST maps from the equatorial Pacific and elsewhere—for ENSO analysis and prediction. Barnston et al. (2012) have ascertained that the real-time EMR forecasts of ENSO indices are highly competitive among the two dozen dynamical and statistical forecasts in the ENSO multimodel prediction plume of the International Research Institute for Climate and Society (IRI), out to over 12 months. Moreover, Chekroun et al. (2011a) have shown that the predictive skill of EMR models can be improved further by taking advantage of the time-dependent properties of the residual noise to perform interannual forecasts of the reduced variables.

Molkov et al. (2012) have independently proposed another way of constructing empirical models suitable for long-term forecasts of the evolution of the system's statistics. In the latter approach, models are constructed as discrete stochastic maps by direct analysis of the time series. These maps present a superposition of stochastic and deterministic components, each of which are functions

of time and of the current state of the system, reconstructed by using artificial neural networks (ANNs).

Molkov et al. (2012) have also shown the ability of their stochastic maps, reconstructed by using scalar time series, to forecast the evolution of the invariant measure generated by discrete stochastic maps, as well as by time-continuous systems of differential equations. In general, and without going into technical details, we mean by an invariant measure a measure defined on the model's phase space that is supported by its attractor and is invariant under the model's governing equations. In particular, the approach of these authors allows one to predict the main bifurcations of the invariant measures of the system under study for times that greatly exceed the duration of the time series being analyzed.

As a first step toward our overall goal, this paper investigates the applicability of the empirical model approach overall, and of the ANN-based methodology of Molkov et al. (2011, 2012) in particular, to forecast critical transitions in simple conceptual ENSO models. Part II deals with more detailed models that include explicit physical-space dependence. The time series used in this paper, which do exhibit critical transitions, were generated by idealized, delay-differential equation (DDE) models with periodic forcing, which represents the seasonal cycle.

The DDE models used here take into account the main conceptual elements responsible for the ENSO phenomenon, as detailed in section 3. Three such models have been analyzed: the Ghil et al. (2008b) model of thermocline depth with one delay, one feedback, and seasonal forcing; and the Tziperman et al. (1994) and Galanti and Tziperman (2000) models for both SST and thermocline depth, which include positive as well as negative feedbacks.

The above-cited studies have shown that these three models, depending on their parameter values, exhibit several dynamic regimes, including periodic behavior with integer period (in units of a year), as well as quasi-periodic and chaotic behavior. Variation of model parameters may cause critical transitions related to switches between these regimes and related, in turn, to abrupt catastrophic changes in the model's statistics.

We have modified each of these three models for the purposes of this study by adding time-dependent trends for the governing parameters, which represent slow changes in the system's state, as well as stochastic noise perturbing the parameter that controls the strength of atmosphere–ocean interaction. We generate a segment of the time series that does not contain qualitative dynamical changes and use it for learning the model's statistics. Having done so, we try next to forecast the critical transitions that occur beyond the learning interval.

The paper is organized as follows. Section 2 describes our general approach to empirical modeling based on random dynamical systems, and a model of the evolution operator that will be used for the forecasts is derived. Section 3 reviews conceptual ENSO models based on DDEs with periodic forcing. Section 4 describes the reconstruction method in the reduced phase space using the time series. The forecast results for the three models are presented in section 5. These results are summarized and discussed in section 6.

2. Empirical modeling using ANNs

To start, we note here that empirical reconstruction of a complex, high-dimensional system—such as the one that governs ENSO—is unavoidably based on an evolution operator acting on a low-dimensional space that is a projection of the original phase space of the full system. In general, such a projection is onto but not one-to-one; that is, two states of the initial system, whether neighboring or far away from each other in the full phase space, may project onto the same state in the reduced phase space. Moreover, this indeterminacy is not homogeneous within the phase space.

The main idea of using empirical models that include random processes is to describe this indeterminacy stochastically. In the approach of Molkov et al. (2012), the stochastic component of the evolution operator depends on the current state of the system; this operator structure effectively takes into account the above-mentioned indeterminacy. Moreover, if the relation between neighboring states is "almost unique," the evolution operator is reconstructed quite accurately. In other words, inclusion of a state-dependent stochastic term into the empirical model helps the latter resolve the behavior on the low-dimensional projection of the full model's higher-dimensional attractor. The present study shows that this approach is indeed effective in forecasting critical transitions in ENSO dynamics.

a. The stochastic model

Let $\{\mathbf{U}(t_n) = \mathbf{U}_n\}_{n=1}^{N}$, with $\mathbf{U}(t) \in \mathbb{R}^d$, represent a sequence of states of a d-dimensional system obtained from an observed time series. Typically $d \ll D$, where D is the dimension of the full system that generated the time series. We assume that the vector process $\mathbf{U}(t)$ is centered and has unit variance [i.e., $\mathbb{E}(\mathbf{U}) = 0$ and $\mathrm{Var}(\mathbf{U}) = 1$, where $\mathbb{E}$ and Var denote mathematical expectation and variance, respectively]. The purpose is to reconstruct the relations between these successive states, that is, to obtain an evolution operator $\varphi\colon \mathbb{R}^d \to \mathbb{R}^d$ acting

on $\mathbf{U}(t)$. In fact, Chekroun et al. (2014) have rigorously shown that, under suitable conditions, a lower-dimensional Markov chain representation of a time-continuous high-dimensional process can capture essential features of the latter.

As mentioned above, even if the evolution operator in the full phase-space $\mathbb{R}^D$ is one-to-one, the corresponding map $\mathbf{U}_n \to \mathbf{U}_{n+1}$ is, in general, not unique. Accordingly, we will proceed with constructing a stochastic evolution operator, defined in Arnold (1998) as

$$\mathbf{U}_{n+1} = \boldsymbol{\varphi}(\boldsymbol{\omega}_n, \mathbf{U}_n), \tag{1a}$$

$$\varphi: \Omega \times \mathbb{R}^d \to \mathbb{R}^d \quad \text{and} \tag{1b}$$

$$\boldsymbol{\omega}_{n+1} = \theta(\boldsymbol{\omega}_n), \tag{1c}$$

$$\theta: \Omega \to \Omega. \tag{1d}$$

Here (Ω, Σ, P) is a probability space, with sample space Ω, algebra of measurable sets (i.e., of "events") Σ, and probability measure P, while θ is an endomorphism: that is, a measure-preserving map of this probability space into itself (Arnold 1998; Ghil et al. 2008a; Chekroun et al. 2011b). To adapt the very general definition given by Eq. (1) to practical usage, let us reduce it to a simpler, coarse-grained form.

First, we can rewrite Eq. (1a), without loss of generality, as

$$\mathbf{U}_{n+1} = \mathbf{f}(\mathbf{U}_n) + \boldsymbol{\eta}(\boldsymbol{\omega}_n, \mathbf{U}_n), \tag{2}$$

where $\mathbf{f}(\mathbf{U}) = \mathbb{E}\{\boldsymbol{\varphi}(\boldsymbol{\omega}, \mathbf{U})\}$ is the mathematical expectation of the random function $\boldsymbol{\varphi}(\boldsymbol{\omega}, \mathbf{U})$, and $\boldsymbol{\eta}(\boldsymbol{\omega}, \mathbf{U}) = \boldsymbol{\varphi}(\boldsymbol{\omega}, \mathbf{U}) - \mathbf{f}(\mathbf{U})$ is the deviation of $\boldsymbol{\varphi}$ from this expectation. The representation in Eq. (2) allows one to explicitly separate the deterministic and random components of the evolution operator $\mathbf{f}$ and $\boldsymbol{\eta}$, respectively.

It is convenient for numerical computations to represent the stochastic component process [i.e., the time series of random-function values $\boldsymbol{\eta}(\boldsymbol{\omega}_n, \mathbf{U}_n)$] as a white Gaussian noise process with state-dependent amplitude. The stochastic term $\boldsymbol{\eta}$ can then be expressed as

$$\boldsymbol{\eta}(\boldsymbol{\omega}, \mathbf{U}) = \hat{\mathbf{g}}(\mathbf{U})\boldsymbol{\zeta}(\boldsymbol{\omega}), \quad \text{where} \quad \hat{\mathbf{g}}: \mathbb{R}^d \to \mathcal{L}_d(\mathbb{R}) \quad \text{and} \quad \boldsymbol{\zeta}: \Omega \to \mathbb{R}^M. \tag{3}$$

Here, the vector $\boldsymbol{\zeta}$ is assumed to have independent, normally distributed components $\{\zeta_l \propto N(0, 1): l = 1, \ldots, d\}$ and to be drawn from a white noise process with Gaussian probability density $w(\boldsymbol{\zeta}) = \mathbb{E}\{\delta[\boldsymbol{\zeta} - \boldsymbol{\zeta}(\boldsymbol{\omega})]\}$. With this assumption, it is natural to restrict the class of matrices $\hat{\mathbf{g}}$ to the set $\mathcal{L}_d(\mathbb{R})$ of non-degenerate lower-triangular matrices of dimension d over the field $\mathbb{R}$; evidently, the set $\mathcal{L}_d(\mathbb{R})$ suffices to determine any covariance matrix $\hat{\mathbf{G}} = \hat{\mathbf{g}}^{\mathrm{T}}\hat{\mathbf{g}}$ of the random term in Eq. (2). Finally, the matrix $\hat{\mathbf{g}}$ is assumed to depend on $\mathbf{U}$; it describes the distribution of the random disturbance intensity in the model's reduced phase space.

The coarse graining in Eq. (3) implies that the processes that affect the time series—but cannot be described by the deterministic part of Eq. (2)—are represented by a random process with short autocorrelation time. Taking Eq. (3) into account, Eq. (2) takes the following form:

$$\mathbf{U}_{n+1} = \mathbf{f}(\mathbf{U}_n) + \hat{\mathbf{g}}(\mathbf{U}_n)\boldsymbol{\zeta}_n. \tag{4}$$

Molkov et al. (2012) showed, by way of example, that such a simplification of the empirical model enables a successful solution of the reconstruction problem, even in the case of a system being reconstructed that has obviously non-Gaussian statistics.

b. Bayesian reconstruction

Equation (4) defines a Markov process with the following transition probabilities:

$$P(\mathbf{U}_{n+1} \,|\, \mathbf{U}_n) = \int \delta[\mathbf{U}_{n+1} - \mathbf{f}(\mathbf{U}_n) - \hat{\mathbf{g}}(\mathbf{U}_n)\boldsymbol{\zeta}_n] w(\boldsymbol{\zeta}_n)\, d\boldsymbol{\zeta}_n, \tag{5}$$

where $w(\boldsymbol{\zeta})$ is the density of ζ. The resulting likelihood function, using the Gaussianity of ζ, is expressed as

$$P(\mathbf{U} \,|\, \mathbf{f}, \hat{\mathbf{G}}) = \prod_n P(\mathbf{U}_{n+1} \,|\, \mathbf{U}_n) \propto \prod_n \frac{1}{|\hat{\mathbf{G}}(\mathbf{U}_n)|^{1/2}} \exp\left\{-\frac{1}{2}[\mathbf{U}_{n+1} - \mathbf{f}(\mathbf{U}_n)]^{\mathrm{T}} \hat{\mathbf{G}}^{-1}(\mathbf{U}_n)[\mathbf{U}_{n+1} - \mathbf{f}(\mathbf{U}_n)]\right\}. \tag{6}$$

According to Bayes's theorem, the posterior distribution P_{post} of the parameters that appear in $\mathbf{f}$ and $\hat{\mathbf{g}}$ is specified, to within a multiplicative factor that does not depend on $\mathbf{f}$ or $\hat{\mathbf{g}}$, by the following expression:

$$P_{\text{post}}(\mathbf{f},\hat{\mathbf{g}}\,|\,\mathbf{U}) \propto P(\mathbf{U}\,|\,\mathbf{f},\hat{\mathbf{g}})P_{\text{prior}}(\mathbf{f},\hat{\mathbf{g}}), \tag{7}$$

where the distribution $P_{\text{prior}}(\mathbf{f}, \hat{\mathbf{g}})$ is determined by prior restrictions on the operator's parameters. The computation and the analysis of $P_{\text{post}}(\mathbf{f}, \hat{\mathbf{g}}\,|\,\mathbf{U})$ in Eq. (7) thereby solves the inverse modeling problem, based on the observed time series $\mathbf{U}(t_n)$.

c. *Inverse modeling: Functional form and parameter values*

The functions $\mathbf{f}$ and $\hat{\mathbf{g}}$ will be understood here as being determined by a prescribed functional form and by the parameters that appear in this form. We assume now that the right-hand side (rhs) in Eq. (4) is well defined over at least some open set of the reduced phase space $\mathbb{R}^d$: that is, that the functional forms of $\mathbf{f}$ and $\hat{\mathbf{g}}$ have been defined in some way over such a set.

We use ANNs (Hornik et al. 1989) to approximate both the vector function $\mathbf{f}$ and the matrix function $\hat{\mathbf{g}}$, as follows:

$$[\mathbf{A}^{d_{\text{out}}}_{m_{d_{\text{in}}}}(\mathbf{U},t)]_k = \sum_{i=1}^{m}(\alpha_{ki}+\beta_{ki}t)\tanh\left(\sum_{j=1}^{d_{\text{in}}} w_{ij}U_j+\gamma_i\right), \quad \text{for} \quad k=1,\ldots,d_{\text{out}}; \tag{8a}$$

$$\mathbf{f}(\mathbf{U},\mathbf{t}) = \mathbf{A}^{d}_{m_{f_d}}(\mathbf{U},\mathbf{t}) \quad \text{and} \tag{8b}$$

$$\text{vec}[\hat{\mathbf{g}}(\mathbf{U},\mathbf{t})] = \mathbf{A}^{d(d+1)/2}_{m_{g_d}}(\mathbf{U},\mathbf{t}). \tag{8c}$$

Here vec[$\hat{\mathbf{g}}$] is the so-called half-vectorization of the lower-triangular matrix $\hat{\mathbf{g}}$: that is, the function that converts this matrix into the vector containing all the elements of the matrix, excluding the zero entries above the main diagonal; d_{in} is the number of ANN inputs; d_{out} is the number of outputs; and m is the number of neurons in the hidden layer, while m_f and m_g are the m values in the deterministic and stochastic terms of Eq. (4), respectively.

In line with the considerations put forth by Neal (1993), we assume Gaussian prior distributions of network parameters of the form

$$P_{\text{prior}}(\boldsymbol{\alpha},\boldsymbol{\beta},\mathbf{w},\boldsymbol{\gamma}) \propto \exp\left\{-\sum_{i=1}^{m}\left[\sum_{k=1}^{d_{\text{out}}}\left(\frac{\alpha_{ki}^2}{2\sigma_\alpha^2}+\frac{\beta_{ki}^2}{2\sigma_\alpha^2}\right) + \sum_{j=1}^{d_{\text{in}}}\left(\frac{w_{ij}^2}{2\sigma_w^2}+\frac{\gamma_i^2}{2\sigma_\gamma^2}\right)\right]\right\}, \tag{9}$$

where $\sigma_\alpha^2 = 1/m$, $\sigma_w^2 = 1$, and $\sigma_\gamma^2 = d$ are the variances of the corresponding parameters. These values reflect the most general a priori assumptions about the spatiotemporal properties of the system under study (Molkov et al. 2011, 2012).

The explicit linear time dependence in Eq. (8a) mimics the system's evolution on a time scale that is slow compared to the characteristic time of change of its internal dynamics, as observed in the time series $\mathbf{U}(t)$; we associate such an evolution with trends in the system's external background. Generally, though, the evolution of the operator in time is nonlinear, even when this background varies linearly. Strictly speaking, the faster such changes, the lesser the validity of the linear assumption, and, hence, the predictability limit is closer. But we can expect this assumption to be helpful for some time interval beyond the observations.

Molkov et al. (2011, 2012) demonstrated that this approach to specifying nonautonomous dynamics makes the resulting model well suited for extrapolating its dynamics over a time horizon that is comparable with the observation interval and allows one to make forecasts of the system's statistical properties over such an interval. Under suitable conditions, these forecasts may include the appearance and approximate timing of critical transitions.

Next, for estimating model parameters, we define the cost function as the posterior probability density (PPD) $P_{\text{post}}(\mathbf{f}, \hat{\mathbf{g}}\,|\,\mathbf{U})$: substituting Eqs. (8) and (9) into Eq. (7), we obtain the resulting density in terms of $\mathbf{f}$ and $\hat{\mathbf{g}}$. In this study, we use P_{post} as a cost function for model learning: the fitted model parameters provide the global maximum of the probability density in Eq. (7). Thus, the algorithm used here to forecast critical transitions has the following four basic steps:

(i) Reconstruction of the phase-space variables $\mathbf{U}(t)$ from an observed time series. The procedure for scalar time series case is described in section 4a. In the multivariate case, a more sophisticated method is proposed in Part II.

(ii) Minimization of the multivariate function $-\log[P_{\text{post}}(\mathbf{f}, \hat{\mathbf{g}}\,|\,\mathbf{U})]$ over the parameters of the functions $\mathbf{f}$ and $\hat{\mathbf{g}}$ in Eqs. (8b) and (8c). We use a quasi-Newtonian, variable-metric method for this [see Press et al. (2002) for details].

(iii) Generating an ensemble of time series using the model governed by Eqs. (4), (8), and (9), as given by the maximum-PPD parameters. This ensemble approximates the most probable behavior of the system for a specified time interval.

(iv) Investigating the changes in the probability density sampled by the above ensemble to determine the occurrence of critical transitions and their timing.

3. DDE models of ENSO variability

The DDE models used here take into account the main conceptual elements responsible for the ENSO phenomenon: (i) the Bjerknes (1969) hypothesis on the existence of a positive feedback as a mechanism for the growth of an internal instability that produces large positive SST anomalies in the eastern tropical Pacific; (ii) the presence of delayed oceanic wave adjustments related to the onset and propagation of Kelvin and Rossby waves [i.e., a negative feedback that compensates for the previous positive feedback and allows a return to colder conditions in the basin's eastern part (Suarez and Schopf 1988)]; and (iii) the existence of seasonal forcing. Further details on these mechanisms are given by Ghil et al. (2008b) and Ghil and Zaliapin (2013). Three such models have been analyzed: the Ghil et al. (2008b) model of thermocline depth with one delay, one feedback, and seasonal forcing; and the Tziperman et al. (1994) and Galanti and Tziperman (2000) models for both SST and thermocline depth, which include positive as well as negative feedbacks.

a. *Initial DDE models*

Starting in the 1980s, the effects of delayed feedbacks and external forcing have been studied using the DDE formalism [see, e.g., Bhattacharya et al. (1982) or Ghil and Childress (1987) for geoscience applications and Hale and Lunel (1993) for DDE theory]. Several DDEs have been suggested as toy models for ENSO variability.

Battisti and Hirst (1989) have considered the linear autonomous DDE:

$$\frac{dT}{dt} = -\alpha T(t-\tau) + T, \quad \text{where} \quad \alpha > 0 \quad \text{and} \quad \tau > 0. \tag{10}$$

Here, T represents the sea surface temperature averaged over the eastern equatorial Pacific. The first term on the rhs of Eq. (10) mimics the negative feedback due to the oceanic waves, while the second term reflects Bjerknes's positive feedback. Battisti and Hirst (1989) have shown that the solutions of this equation reproduce some of the main features of a fully nonlinear coupled atmosphere–ocean model of ENSO dynamics in the tropics (Zebiak and Cane 1987; Battisti 1988).

Suarez and Schopf (1988) and Battisti and Hirst (1989) also studied a nonlinear version of Eq. (10), in which a cubic nonlinearity is added to the rhs of the equation:

$$\frac{dT}{dt} = -\alpha T(t-\tau) + T - T^3, \quad \text{where} \quad 0 < \alpha < 1 \quad \text{and} \quad \tau > 0. \tag{11}$$

This system has three steady states, obtained by finding the roots of the polynomial on the rhs:

$$T_0 = 0 \quad \text{and} \quad T_{\pm} = \pm(1-\alpha)^{1/2}.$$

The so-called inner solution T_0 is always unstable, while the outer solutions $T_{\pm}$ may be stable or unstable, depending on the parameters (α, τ). If an outer steady state is unstable, the system exhibits bounded oscillatory dynamics. Suarez and Schopf (1988) showed numerically that a typical period of such oscillatory solutions is about twice the delay τ.

The delay equation idea was very successful in explaining the periodic nature of ENSO events. Indeed, the delayed negative feedback does not let a solution fade away or blow up, as in the ordinary differential equation case with $\tau = 0$; it thus gives rise to an internal oscillator whose period depends on the delay and the particular form of the equation's rhs. DDE modeling has also emphasized the importance of nonlinear interactions in shaping the complex dynamics of the ENSO cycle. At the same time, many important details of ENSO variability still had to be explained.

First, a delayed oscillator similar to Eq. (10) or Eq. (11) typically has periodic solutions with well-defined periods. However, the occurrence of ENSO events is irregular and can only be approximated very coarsely by a periodic function. Second, El Niño events always peak during the Northern Hemisphere (boreal) winter; hence their name. Such phase locking cannot be explained by a purely internal delayed oscillator. Third, the value of the period produced by the delay equations deviates significantly from actual ENSO recurrence times of 2–7 yr. The delay τ, which is the sum of the basin transit times of the westward Rossby and eastward Kelvin waves, can be roughly estimated to lie in the range of 6–8 months. Accordingly, the model of Eq. (11) suggests a period of 1.5–2 yr, at most, for the repeating warm events; this is about half the dominant ENSO recurrence time.

b. *Tziperman et al. model*

The next important step in developing ENSO modeling in the DDE framework was made by Tziperman et al. (1994), who demonstrated that the above discrepancies can be removed by considering nonlinear interactions between the internal oscillator and the external periodic forcing of the tropical Pacific by the seasonal cycle. These authors also introduced a more realistic type of nonlinear coupling between atmosphere and ocean to reflect the fact that the delayed negative feedback saturates as the absolute value of the key dependent variable T increases; note that in Eq. (10) the

feedback is linearly proportional to the delayed state variable $T(t-\tau)$.

Münnich et al. (1991) studied an iterated-map model of ENSO and compared in detail cubic and sigmoid nonlinearities. As a result, Tziperman et al. (1994) chose the sigmoid type of nonlinearity and thus formulated the periodically forced, nonlinear DDE:

$$\frac{dT}{dt} = -\alpha \tanh[\kappa T(t-\tau_1)] + \beta \tanh[\kappa T(t-\tau_2)] + \gamma \cos(2\pi\omega t). \quad (12)$$

Here, the first term on the rhs represents the westward-traveling Rossby wave, the second term represents the eastward Kelvin wave, and the last one is a seasonal forcing. The parameters α, β, and γ represent the relative strengths of these three driving forces; τ_1 and τ_2 are Rossby and Kelvin wave delays, respectively; and κ represents the strength of the atmosphere–ocean coupling. The period of the seasonal forcing, $1/(2\pi\omega)$], is one year, and we will take $\omega = 1$ hereafter, for simplicity.

Depending on the parameter values, the model of Eq. (12) was shown to have solutions that possess an integer period, are quasiperiodic, or exhibit chaotic behavior. The increase of solution complexity—from period one to an integer but higher period, and on to quasiperiodicity and chaos—is caused by the increase of the atmosphere–ocean coupling parameter κ. Tziperman et al. (1994) also demonstrated that this forced DDE system exhibits period locking, when the external, "explicit" oscillator wins the competition with the internal, delayed one, causing the system to stick to an integer period; dependence of the system's period on model parameters takes the form of a devil's staircase.

This result is in agreement with a growing body of work (Ghil and Robertson 2000; Chang et al. 1994, 1995; Jin et al. 1994, 1996; Tziperman et al. 1994, 1995) that points to resonances between the Pacific basin's intrinsic air–sea oscillator and the annual cycle as a possible cause for the tendency of warm events to peak in boreal winter, as well as for ENSO's intriguing mix of temporal regularities and irregularities. For example, Jin et al. (1994, 1996) provide a more detailed analysis of phase locking in an intermediate coupled ENSO model.

These and other ENSO studies with DDE models have been limited to (i) the linear stability analysis of steady-state solutions, which are not typical in forced systems; (ii) case studies of particular trajectories; or (iii) one-dimensional scenarios of transition to chaos, where one varies a single parameter, while the others are kept fixed. A major obstacle for the complete bifurcation and sensitivity analysis of such DDE models lies in the complex nature of DDEs, whose numerical and analytical treatment is harder than that of models with no delays.

c. *Ghil et al. model*

Ghil et al. (2008b) and Zaliapin and Ghil (2010) took several steps toward a comprehensive analysis, numerical as well as theoretical, of DDE models relevant for ENSO phenomenology. These authors considered a simplified version of Eq. (12):

$$\frac{dT}{dt} = -\tanh[\kappa T(t-\tau)] + b\cos(2\pi t), \quad (13)$$

and, for the first time, performed its analysis in the complete 3D space of the physically relevant parameters: strength of seasonal forcing b, ocean–atmosphere coupling κ, and transit time τ of oceanic waves across the tropical Pacific.

This model reproduces many aspects of ENSO phenomenology. These aspects include prototypes of El Niño and La Niña events; intraseasonal activity reminiscent of Madden–Julian oscillations (Madden and Julian 1994) or westerly wind bursts; and spontaneous interdecadal oscillations. The model also provided a good justification for the observed quasi-biennial oscillation in tropical Pacific SSTs and trade winds (Philander 1990; Diaz and Markgraf 1992; Jiang et al. 1995; Ghil et al. 2002): in this model, ENSO's 2–3-yr period arises naturally as the correct multiple (4 times) of the sum of the basin transit times of Kelvin and Rossby waves.

Zaliapin and Ghil (2010) found regions of stable and unstable solution behavior in the model's parameter space; these regions have a complex and possibly fractal distribution of solution properties. The local continuous dependence theorem evoked by Zaliapin and Ghil (2010) suggests that the complex discontinuity patterns indicate the presence of a rich family of unstable solutions that point, in turn, to a complicated attractor.

A simple DDE model like Eq. (13), with a single delay, does reproduce the devil's staircase scenario documented in other ENSO models, including intermediate coupled models and GCMs, as well as in observations (Jin et al. 1994; Tziperman et al. 1994; Ghil and Robertson 2000). The latter result suggests that interdecadal variability in the extratropical, thermohaline circulation (Dijkstra and Ghil 2005) might interfere constructively with ENSO's intrinsic variability on this time scale. Zaliapin and Ghil (2010) found that the model of Eq. (13) is characterized by phase locking of the solutions' local extrema to the seasonal cycle; in particular, solution maxima (i.e., model El Niños) tend to occur in boreal winter.

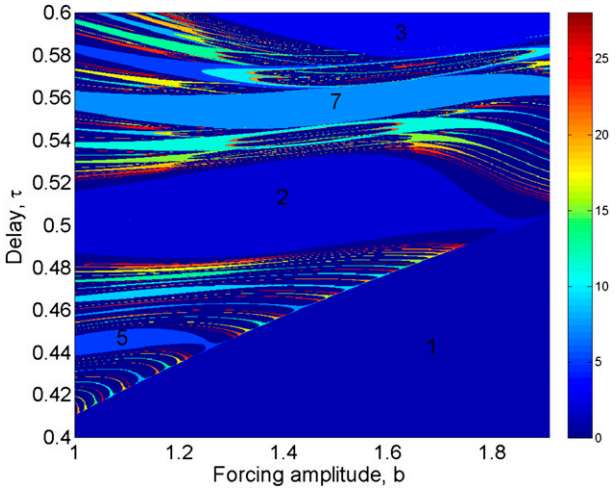

FIG. 1. Period map for the delayed coupled oscillator of Eq. (13). The figure shows the period P as a function of two model parameters: amplitude b of seasonal forcing and delay τ of the oceanic waves; the ocean–atmosphere coupling strength is fixed at $\kappa = 10$. Aperiodic solutions correspond to $P = 0$. Numbers indicate the period values within the largest constant-period regions. From Ghil et al. (2008b).

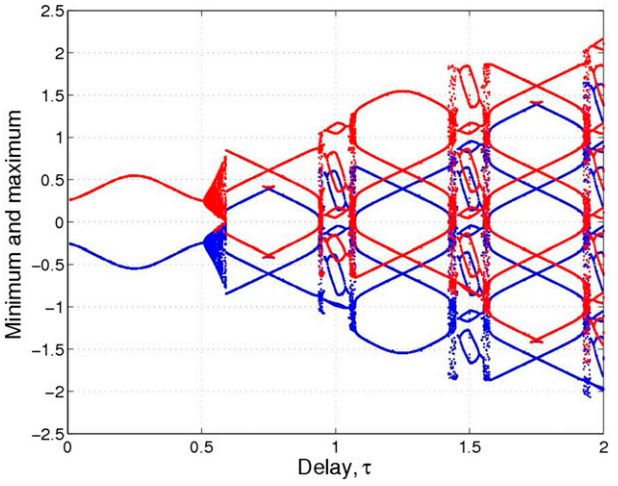

FIG. 2. Local maxima (red) and minima (blue) of solutions of Eq. (13) as a function of delay τ; the other parameter values are fixed at $\kappa = 10$ and $b = 2$. Notice the aperiodic regimes between periodic windows of gradually increasing period. This figure corresponds to the rightmost vertical section of the region shown in Fig. 1; from Zaliapin and Ghil (2010).

These authors also found multiple solutions coexisting for physically relevant values of the model parameters. Figure 1 illustrates the model's sensitive dependence on parameters in a region that corresponds roughly to actual ENSO dynamics. The figure shows the behavior of the period P of model solutions as a function of two parameters: the propagation period τ of oceanic waves across the tropical Pacific, and the amplitude b of the seasonal forcing; for aperiodic solutions, one sets $P = 0$. Although the model is sensitive to each of its three parameters (b, κ, τ), sharp variations in P are mainly associated with changing the delay τ, which is plotted on the ordinate.

This sensitivity is an important qualitative conclusion, since in reality the propagation times of Rossby and Kelvin waves are affected by numerous phenomena that are not related directly to ENSO dynamics. The sensitive dependence of the period on the model's parameters is consistent with the irregularity of occurrence of strong El Niños and can help explain the difficulty in predicting them (Latif et al. 1994; Ghil and Jiang 1998).

The model's instabilities disappear, and the dynamics of the system becomes purely periodic, with a period of one year (not shown), as soon as the atmosphere–ocean coupling κ vanishes or the delay τ decreases below a critical value. Figure 2 illustrates this effect in greater detail: the period P of model solutions increases with τ in discrete jumps ($P = 2k + 1, k = 0, 1, 2, \ldots$) separated by narrow, apparently chaotic "windows" in τ. This increase in P is associated with the increase of the number of distinct local extrema, all of which tend to occur at the same position within the seasonal cycle. The alternation between regular and chaotic windows resembles, in fact, the behavior of chaotic dynamical systems in discrete time (Kadanoff 1983) and suggests that the model's aperiodic dynamics is, in fact, chaotic.

This chaotic behavior implies, in particular, that small perturbations in the model parameters or in initial states may lead to significant changes of the model dynamics. Because of this sensitive dependence, forecasting the model's behavior, as well as that of the related natural phenomenon, is a hard problem. The boundary between the domains of stable and unstable model behavior is clearly visible at the lower right of Fig. 1.

The period-1 region below and to the right of this boundary contains simple solutions that change smoothly with the values of model parameters. The region above and to the left is characterized by sensitive dependence on parameters. The range of parameters that corresponds to present-day ENSO dynamics lies on the border between the model's stable and unstable regions. Hence, if the dynamical phenomena found in the model have any relation to reality, tropical Pacific SSTs and other fields that are highly correlated with them, inside and outside the tropics, can be expected to behave in an intrinsically unstable manner; they could, in particular, change quite drastically with global warming.

d. Galanti and Tziperman model

Galanti and Tziperman (2000) emphasized that understanding of the physical mechanisms of ENSO's phase locking requires exploration of idealized models

that are more rigorously derived than the Tziperman et al. (1994) model, reproduced in Eq. (12) here, yet still simple enough to allow detailed exploration. Accordingly, the paper under discussion investigated the interaction between ENSO oscillations and the seasonal cycle using several carefully derived models. We review here briefly the model for the so-called mixed-mode regime, which is based on the recharge oscillator of Jin (1997a,b).

Unlike the original model of Tziperman et al. (1994), Galanti and Tziperman (2000) explicitly consider the Kelvin waves and formulate the model as a delayed-oscillator equation for SST in the eastern tropical Pacific. Hence, both oceanic wave time scales and thermodynamic time scales play a role in this model. Finally, the model expresses the thermocline depth anomaly $h(t)$ at the eastern edge of the basin via the earlier values of $h(s)$ and of the equatorial SST $T(s)$ for $s < t$:

$$h(t) = e^{-\epsilon(\tau_1+\tau_2)} r_W r_E h(t-\tau_1-\tau_2) - e^{-\epsilon\tau_2} r_W \frac{1}{\beta\rho} A\delta\tau_1 \mu(t-\tau_2-\tau_1/2)$$
$$\times e^{-\epsilon\tau_1/2} bT(t-\tau_2-\tau_1/2) + e^{-\epsilon\tau_2/2} \frac{1}{\rho C_0} \delta\tau_2 b\mu(t-\tau_2/2)T(t-\tau_2/2) \quad \text{and} \tag{14a}$$

$$\partial_t T = -\epsilon_T - \frac{2w}{3H}[T - T_{\text{sub}}(h)]. \tag{14b}$$

In Eq. (14a), the first term represents the free Rossby and Kelvin waves, the second represents the excited Rossby wave, and the third represents the excited Kelvin wave. The ocean dynamics is modeled here using the following parameters: ϵ is the oceanic damping coefficient; H is the mean thermocline depth and $C_0 = (g'H)^{1/2}$, where g' is the reduced-gravity acceleration; τ_1 is the time it takes a Rossby wave to cross a basin of length L; $\tau_2 = L/C_0$ is the time it takes a Kelvin wave to cross the same basin; $\delta = 1/2$ is the fraction of crossing time during which the wind stress affects the oceanic waves; and r_W and r_E are reflection coefficients at the western and eastern boundaries, respectively.

The thermodynamic parameterization in Eq. (14b) uses the thermal damping coefficient ϵ_T, the mean upwelling w, and the temperature anomaly $T_{\text{sub}}(h)$ at depth H. Finally, the ocean–atmosphere interaction involves two parameters: the coupling coefficient μ between equatorial SST and wind stress, and the mean annual coupling strength b. The seasonal forcing enters into this model via the parameter μ, which varies according to

$$\mu = 1 + \epsilon\cos(w_a t - \phi).$$

Numerical values of all these parameters appear in Galanti and Tziperman (2000, their Table 1). The model of Eq. (14) is nonlinear because of the sigmoid shape of the function $T_{\text{sub}}(h)$.

The main focus of the Galanti and Tziperman (2000) analysis was understanding the mechanism of the well-known phase locking of ENSO events to boreal winter. Most notably, all model variants they considered exhibited strong phase locking, with warm events peaking during boreal winter. Still, an event peak could shift by about 2 months as a result of the adjustment time of temperature T to changes in thermocline depth h.

Finally, Galanti and Tziperman (2000) considered linear versions of the three models analyzed in their study and concluded that ENSO's phase locking is not a result of model nonlinearity. Instead, it is as a result of the seasonal modulation of the model parameters, and it can be observed in linearized models as well. This conclusion is entirely consistent with the classical analysis of parametric forcing in the linear Mathieu equation, obtained by linearizing the Hill equation of lunar-motion theory (Abraham and Marsden 1987).

4. Empirical model reconstruction

a. Periodic forcing and embedding

To study predictability of the critical transitions in ENSO dynamics using the approach of section 2, we use time series generated by the model of Eqs. (12), (13), and (14) that were described in section 3. One of each model's parameters is changed adiabatically (i.e., on a time scale that is slow compared to the model's internal variability). Such a slow, prescribed evolution allows us to produce time series that include critical transitions.

Specifically, we use a linear time dependence of a governing parameter $\rho(t)$ say:

$$\rho(t) = \rho(0) + [\rho(N) - \rho(0)]\frac{t}{N}, \tag{15}$$

where N is the duration of the time series being studied.

An important step in empirical modeling of the evolution operator is choosing a learning sample. This step includes reconstructing the phase variables $X \in \mathbb{R}^d$ using

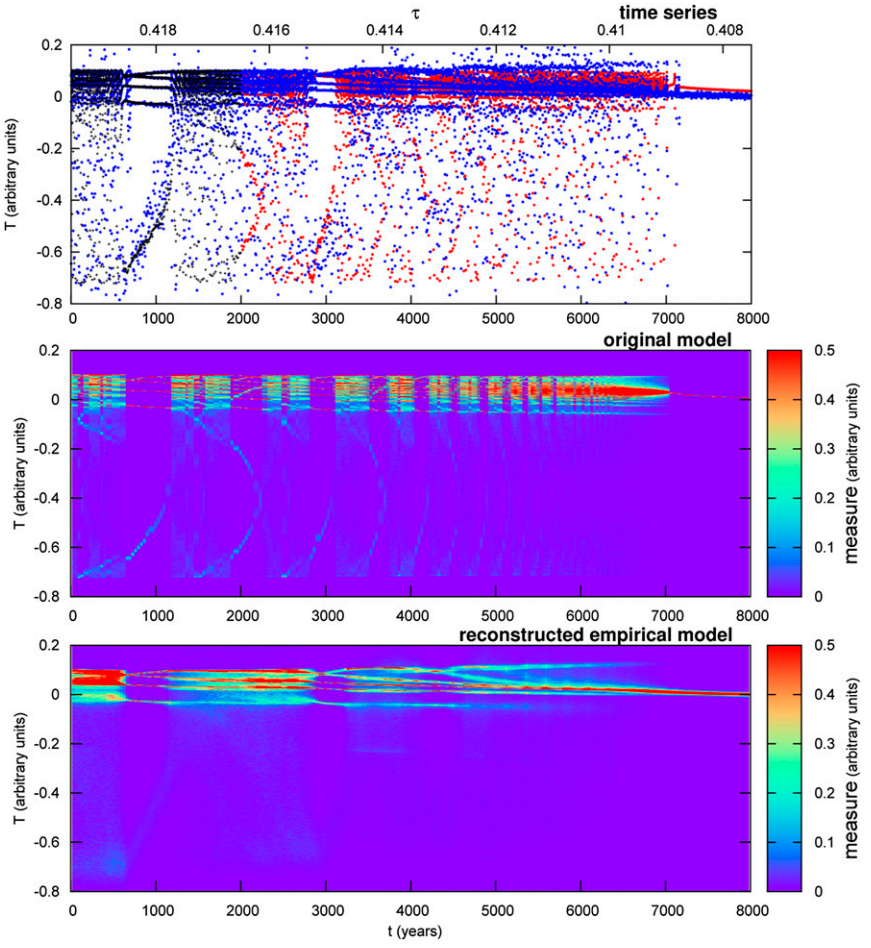

FIG. 3. Reconstruction of the Ghil et al. (2008b) model's behavior; the model version studied here is governed by Eq. (13) with the parametric forcing of Eqs. (15) and (16). (top) The observed (black) and future (red) behavior of the original model; the abscissa is time t running from 0 to 8000. The empirical model's training interval is $N_{tr} = 2000$, which corresponds to the delay in the dynamical model changing over the range $0.4195 \leq \tau_{learn} \leq 0.4165$, and the noise level in Eq. (16) is $\sigma = 0.03$. The empirical model dynamics is shown in blue; its dimension is $d = 2$, while the number of parameters in the deterministic and stochastic part, respectively, is $m_f = 10$ and $m_g = 10$. The time-varying PDFs of the (middle) original dynamical model and of (bottom) the empirical reconstructed model are shown; the density scale is shown by the color bars on the right-hand side. See text for details on the invariant measures and their corresponding densities.

a time series $x(t)$, where d denotes the dimension of the reduced phase space under consideration. In this study, the phase variables were obtained using the Mañe–Takens embedding theorem (Mañe 1981; Takens 1981); that is, the values of the time series $x(t)$ were shifted $d - 1$ times by a lag q: $X_i(t) = x[t + q(i - 1)]$, $i = 1, \ldots, d$.

The choice of the lag q will, in general, affect the attractor's projection onto $\mathbb{R}^d$; hence, q should be optimized, along with d and the number of neurons entering the model. In the present study, these parameters were chosen for each time series to achieve the best correspondence between the resulting models and the analyzed time series. The details of this optimization procedure will be discussed in a separate work.

The presence of the annual seasonal cycle has to be taken into account when constructing an empirical ENSO model. This means that the phase space of the analyzed system can be represented as a cylinder, and it is convenient to construct the evolution operator using the Poincaré projection: that is, to model the relations between states separated by 1-yr intervals. Hence, we will construct a discrete evolution operator φ: $\mathbf{X}(t) \rightarrow \mathbf{X}(t + \Delta t)$, where $\Delta t = 1$ yr. The learning, or training, sample is given by $\{\mathbf{X}^n$: $\mathbf{X}(n\Delta t$: $n = 1, \ldots, N_{tr})\}$ where

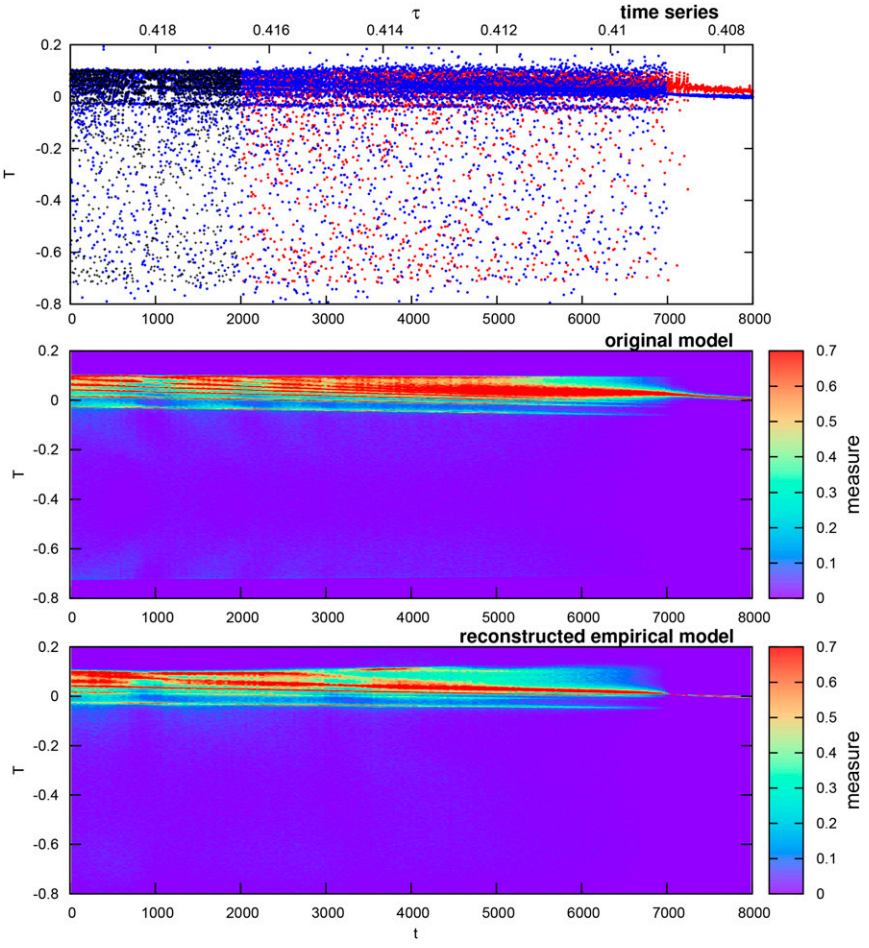

FIG. 4. As in Fig. 3, but with noise level $\sigma = 0.27$.

$\mathbf{X} \in \mathbb{R}^d$ and N_{tr} is the length of the training interval, in years.

b. *Randomized parameters*

The main problem using the time series generated by the deterministic, dynamic models governed by Eqs. (12)–(14) in order to learn an empirical, stochastic model of type Eq. (4) is the lack of sufficient information in these series. Specifically, for physically meaningful values of the pertinent parameters, these models exhibit three types of behavior: (i) periodic oscillations, the period of which is commensurable with the period of the external forcing; (ii) quasi-periodic oscillations that correspond to a dense coverage of a torus in the system's phase space; and (iii) deterministically chaotic variability (Jin et al. 1994, 1996; Tziperman et al. 1994; Ghil et al. 2008b; Galanti and Tziperman 2000; Zaliapin and Ghil 2010). Hence, all critical transitions related to the change of a control parameter represent switches between two of these three states.

Reconstruction of a dynamical-model trajectory from a time series within some fixed regime corresponds to finite sampling of its states from the attractor associated with that particular, asymptotic regime. To predict transition to a different attractor, associated with another regime, the empirical model has to reconstruct the evolution of the Lyapunov exponents responsible for the attractor's stability. It is clear, however, that in the absence of transition processes in the learning sample, one cannot draw any conclusions about the attractor's stability without additional information about the system.

At the same time, the purely deterministic ENSO modeling discussed so far is clearly an idealization, since the observed time series cannot be fully described by purely deterministic equations. In other words, in reality one always observes transient dynamics rather than an asymptotic, stationary regime.

This state of affairs motivates us to modify the models of Eqs. (12) and (13) by adding Gaussian red noise to the

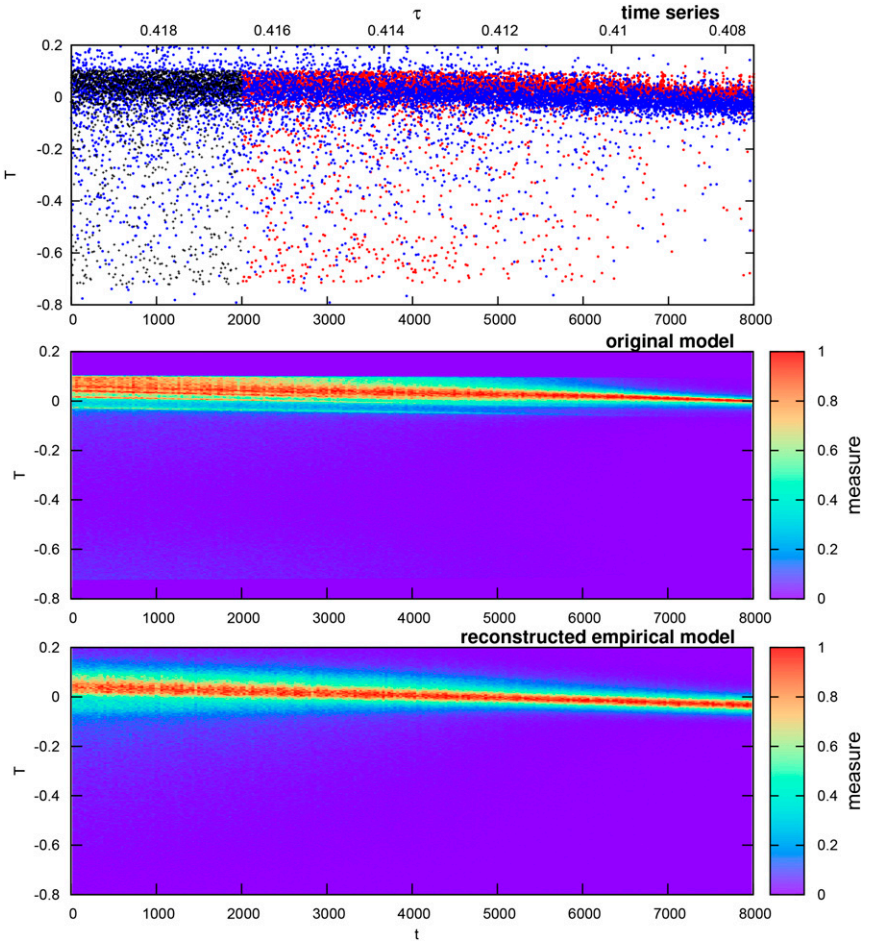

FIG. 5. As in Fig. 3, but with noise level $\sigma = 0.4$.

parameter κ that describes the strength of atmosphere–ocean coupling:

$$\kappa = k(1 + \sigma y) \quad \text{and} \tag{16a}$$

$$dy = -aydt + (2a)^{1/2} dW. \tag{16b}$$

Here, a is a damping parameter for the red noise process y, chosen so that its autocorrelation time is much shorter than the characteristic time of the deterministic model dynamics, thus making the red noise above almost white, while W is a Wiener process and σ^2 multiplies the variance of y. These modified models were used to generate weakly nonstationary time series for different noise levels σ in Eq. (16a).

A different situation is observed for the Galanti and Tziperman (2000) model, governed by Eq. (14), which exhibits chaotic behavior in the parameter range we study here. Such behavior is very informative for reconstructing a system's dynamical properties. In this model, the change of the delay τ_1 gives rise to the creation and destruction of chaotic attractors. We restricted, therefore, this model's analysis to learning within a chaotic regime and did not modify the original Eq. (14) by stochastic perturbations.

5. Predictability results

a. *Ghil et al. model*

The time series produced by the model of Eq. (13), with fixed parameters $k = 100$, $b = 1$, and $a = 25$ and with additional forcing according to Eqs. (15) and (16), are shown in the top panels of Figs. 3–6 . All time series are plotted as yearly dots, according to the Poincaré projection introduced in section 4a; using lines would make the figures illegible. The first three figures correspond to a slow decrease of the delay from $\tau = 0.4195$ to 0.4075, while time, $0 \le t \le 8000$, is in units of 1 yr. The learning interval is $0 \le t \le N_{\text{tr}}$, with $N_{\text{tr}} = 2000$ (shown by the black line in the three top panels of Fig. 7) and the noise has three levels—$\sigma = 0.03$, 0.27, and 0.4—in Figs. 3–5, respectively.

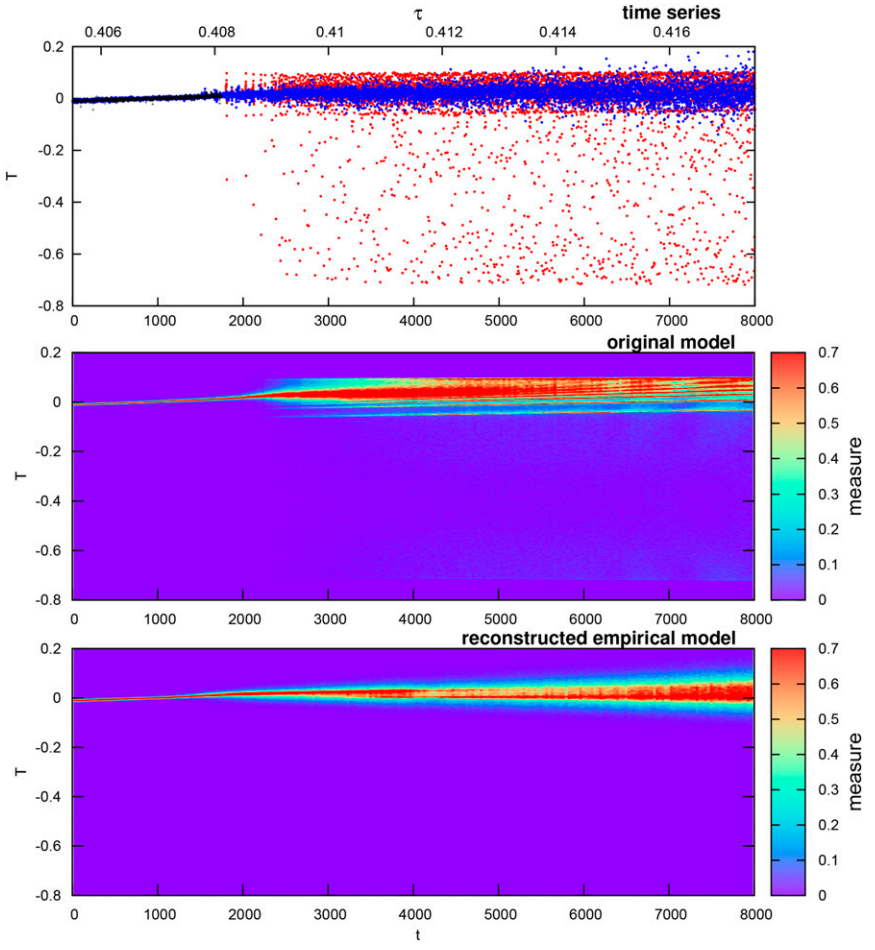

FIG. 6. Reconstruction of the Ghil et al. (2008b) model's behavior in a more difficult-to-predict situation; see text for details. The training interval now is $N_{\rm tr} = 1750$, with noise level $\sigma = 0.27$ and change of the delay over the range $0.4055 \leq \tau_{\rm learn} \leq 0.4081$. Panels and color conventions as in Figs. 3–5.

In Fig. 3 (top panel), the original, dynamical model (red dots outside the learning interval)—with noise level $\sigma = 0.03$ in the time-dependent forcing [cf. Eq. (16a)]—generates clear critical transitions at $t \simeq 800$, 2900, and 7000. The transitions represent changes in the dynamical model's behavior; the last one corresponds to an abrupt decrease in the mean-square fluctuation of the model dynamics. The second and third transitions happen outside of the learning interval, and the last one is located far away from the end of this interval. Note, however, that the second transition, near $t \simeq 2900$, resembles quite well the one that occurs within the learning interval, near $t \simeq 800$, and even the third one includes model behavior that seems to lie within the phase-space domain explored during the learning interval.

At the noise level $\sigma = 0.27$ (Fig. 4), only the last critical transition is noticeable. Finally, for $\sigma = 0.4$ (Fig. 5), the transitions practically disappear.

We used the initial segments, $0 \leq t \leq 2000$, of the dynamical-model solutions in the top panels of Figs. 3–5 to construct an empirical, ANN-based model of Eq. (7) with evolution operator given by Eqs. (4) and (8). The empirical state vector $\mathbf{U}$ here has dimension $d = 2$ and the number of neurons is $m_f = 10$ and $m_g = 10$ in the deterministic and stochastic terms, respectively. The time series generated by the empirical model of Eq. (4), with parameters that maximize the PPD in Eq. (7), are shown in blue in the top panels. Clearly there is good agreement between the red dots (i.e., the dynamical model's behavior targeted for prediction) and the empirical prediction given by the blue dots.

In addition to the time series themselves, we compare the invariant measures of the dynamical and the empirical model at different epochs of t. Rigorously speaking, these invariant measures are supported, when the system's forcing or parameters are time-dependent,

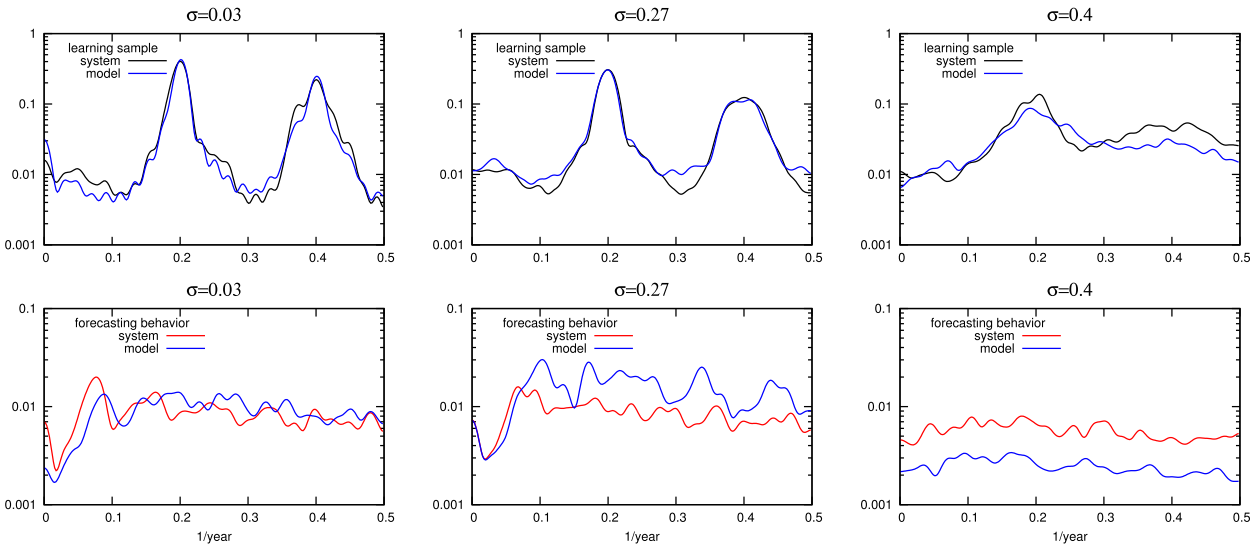

FIG. 7. Fourier spectra for the Ghil et al. (2008b) model, governed here by Eqs. (13), (15), and (16). The noise levels are σ = (left) 0.03, (center) 0.27, and (right) 0.4 in Eq. (16) (i.e., corresponding to Figs. 3–5). (top) The Fourier spectra of the original dynamical (black) and empirical (blue) model for the learning interval $0 \leq t \leq 2000$; (bottom) the spectra of the future behavior of the former (red) and the latter (blue) model for $6000 \leq t \leq 8000$.

by a so-called pullback attractor (Arnold 1998; Ghil et al. 2008a; Chekroun et al. 2011b; Ghil 2015). It is laborious to approximate accurately such a time-dependent attractor, and the invariant measure it supports, when the dynamical system is infinitely dimensional, as in the case at hand.

Instead of following the general procedure outlined in the above references for such a time-dependent attractor, we note that time t enters explicitly into the control parameter $\rho(t)$ in the dynamical model [cf. Eq. (15)], as well as into the parameterization of the ANN model in Eq. (8), and that the time dependence of the parameter ρ is slow. Hence, we generated very long time series—containing approximately 10^5 points each, after skipping the transient of about 10^4 points—of the dynamical model at a fixed value of $\rho(t)$ and of the empirical model at the corresponding value of t in Eq. (8), as a reasonably accurate way of approximating the probability density functions (PDFs) associated with the hypothetical pullback attractor. Indeed, such a PDF, in turn, approximates the density of the invariant measure on the models attractor at epoch t. Then we compared the PDFs so obtained for both dynamical and empirical models as functions of t.

This comparison is illustrated in the middle and bottom panels of Figs. 3–5. The resolution used in these figures suffices to reflect the very thin support of the invariant measure. Increasing the resolution, along with the number of points in the time series, leaves the PDFs visually unchanged. There is also fairly good agreement between the invariant measures associated with the dynamical and the empirical model in Fig. 3 up to $t \simeq 3000$ and again for the final collapse of the variance past $t \simeq 7000$. The agreement becomes gradually less good in Figs. 4 and 5, but the variance collapse past $t \simeq 7000$ is still quite clear in the former.

This collapse is induced by a bifurcation in the unperturbed model of Eq. (13), which manifests itself by destroying an invariant torus in the model's phase space, while replacing it by a stable limit cycle with a 1-yr period; the latter corresponds to one stable fixed point in the discrete Poincaré map. The suddenness of this transition apparently helps the empirical model predict it, as compared with other transitions considered below.

We conclude, therewith, that the proposed Bayesian ANN model of Eq. (8) gives an adequate description of the original model governed by Eqs. (13), (15), and (16), especially at moderate noise levels σ. The empirical model allows one to forecast the behavior of the dynamical one, including its future critical transitions, at least to a certain degree.

In addition, we compared the Fourier spectra of the dynamical and the empirical model within the learning interval and beyond. Given the length of the time series, their Fourier spectra could be computed accurately enough simply by using the windowed Blackman–Tukey correlogram (see Ghil et al. 2002). The spectra so obtained and plotted in Fig. 7 show mostly the presence or absence of two major modes of ENSO variability (Jiang et al. 1995): a quasi-quadriennial (QQ) oscillation

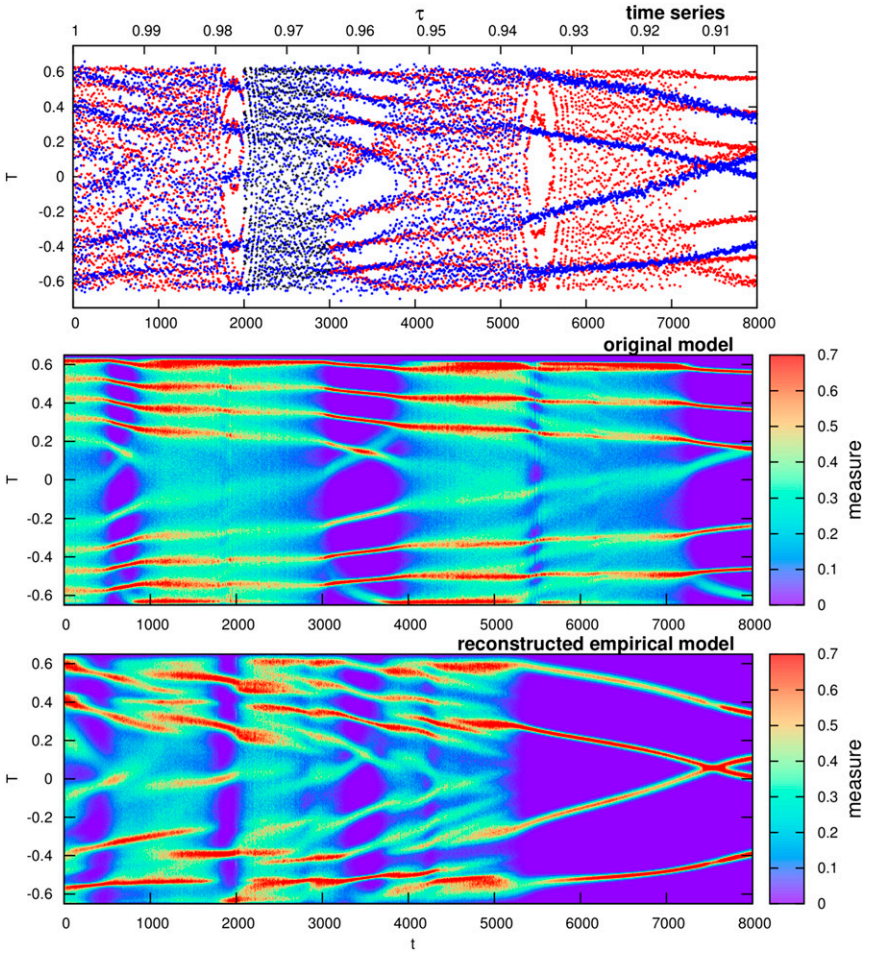

FIG. 8. Reconstruction of the Tziperman et al. (1994) model's behavior, governed here by Eqs. (12), (15), and (16). Panels and color conventions as in Figs. 3–6. The learning interval now has a length of $N_{tr} = 1000$, and the model's forcing parameters are $0.976 \leq \beta_{learn} \leq 0.964$, with noise level $\sigma = 0.05$. The empirical model has dimension $d = 2$, and the parameter numbers are $m_f = 7$ for the deterministic part and $m_g = 2$ for the stochastic part, respectively.

around 0.25 cycles yr^{-1} and a quasi-biennial (QB) one around 0.4 cycles yr^{-1}.

Both the QQ and the QB modes are very energetic for $\sigma = 0.03$ and 0.27 during the learning interval, while for $\sigma = 0.4$ the QQ mode is still quite significant but the QB one has largely disappeared. This disappearance implies that larger stochasticity levels lie outside the range of model validity for ENSO simulation and prediction. During the forecasting interval, both the QQ and QB modes are by-and-large absent, for all σ values. Figure 7 thus indicates good agreement between the dynamical and the empirical model in the spectral domain.

Figure 6 corresponds to a slow increase of the delay from $\tau = 0.4055$ to 0.4175, with the solutions displayed over the same total interval of 8000 yr but an even shorter training interval of $N_{tr} = 1750$ yr; the noise level $\sigma = 0.27$ in the coupling parameter κ is the same as in Fig. 4 above. This situation differs from the one studied in Figs. 3–5, in which—as the delay changes from $\tau = 0.4195$ to 0.4075—the dynamical model evolves during the training interval in the same region of phase space in which it will be located after the upcoming bifurcation, a state of affairs that allows us to adequately forecast the critical transition.

In the present situation, however, there are phase-space regions that the dynamic model visits at later times but not during the learning interval. To forecast a transition associated with totally unobserved behavior in a purely deterministic model with no noise is impossible. The presence of relatively strong noise, however, allows us to forecast, albeit with limited accuracy, such a transition in a stochastically perturbed model.

This is what we see in Fig. 6: the critical transition is located outside the learning interval, and it is predicted

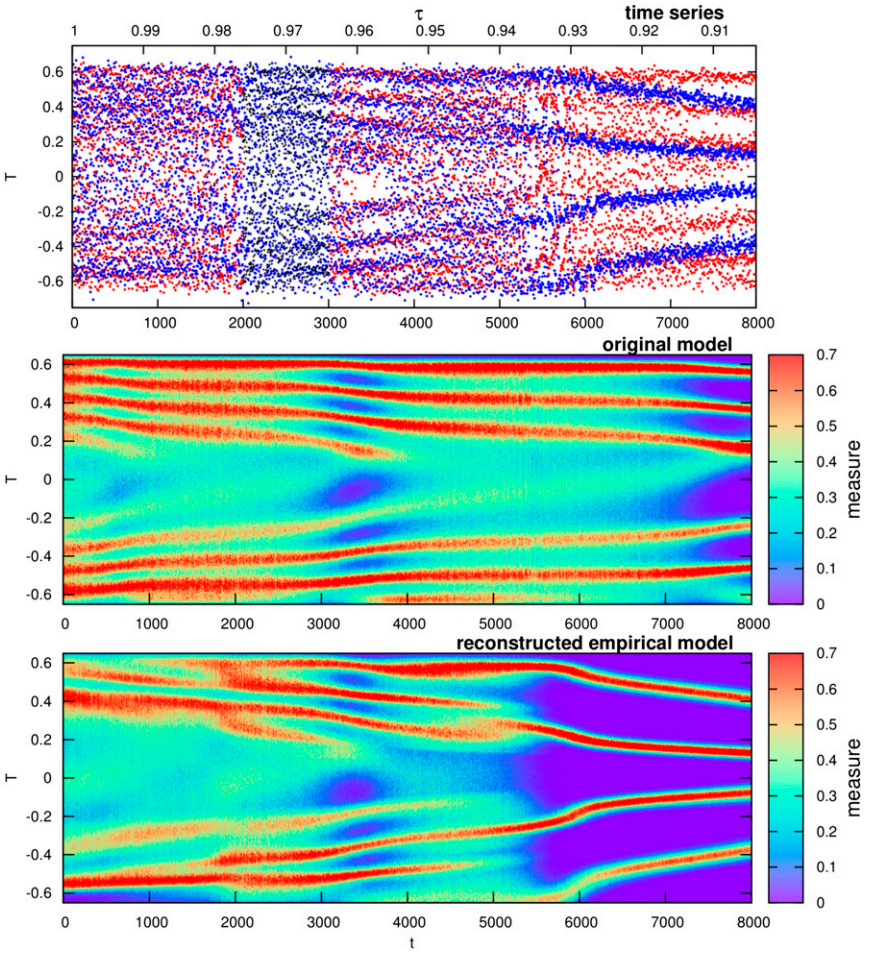

FIG. 9. As in Fig. 8, but with noise level $\sigma = 0.15$.

not as a sharp jump but as a smooth transition in the inverse model's behavior.

b. *Tziperman et al. model*

Figures 8–10 show the time series generated by the model governed here by Eqs. (12), (15), and (16), with parameters $\alpha = 1.1$, $\gamma = 1$, $\tau_1 = 0.6$, $\tau_2 = 0.2$, and $k = 7$, while the control parameter β in Eq. (12) decreases from $\beta(0) = 1$ to $\beta(N) = 0.904$, and the noise levels are $\sigma = 0.05$, 0.15, and 0.3, respectively. The empirical model of the evolution operator has dimension $d = 2$, while the neuron numbers are $m_f = 7$ and $m_g = 2$. These lower values of the neuron numbers, in the deterministic and even more so in the stochastic term of Eq. (4), are sufficient to capture this dynamical model's simpler behavior, as we shall see forthwith.

The training interval here is $2000 \le t \le 3000$, and thus $N_{\rm tr} = 1000$. Figures 8 and 9 demonstrate that, for the noise levels $\sigma = 0.05$ and 0.15, the empirical model's predictability range extends into the past, with β increasing, all the way to $t \simeq 0$ and into the future, with β decreasing, out to $t \simeq 6000$. Over the interval $0 \le t \le 6000$, the empirical model nicely approximates the behavior of the system and successfully forecasts all critical transitions, when $\sigma = 0.05$ or 0.15. When the noise level increases further, to $\sigma = 0.3$ (Fig. 10), the time interval over which the empirical model simulates and predicts adequately the behavior of the dynamical model extends at least as far as the entire interval under consideration (i.e., $0 \le t \le 8000$).

Fourier spectra of the dynamical-model behavior are presented in Fig. 11, in black for the learning interval and in red for the future. Note that here the QQ mode dominates for all three noise levels shown (top panels of the figure), while the QB peak almost disappears in future behavior (bottom panels). Note that QB peak becomes very small at the noise level of $\sigma = 0.3$, so the model with higher noise tends to no longer capture ENSO-like oscillations. Confirmation of the empirical model's skill is given by the close agreement of its

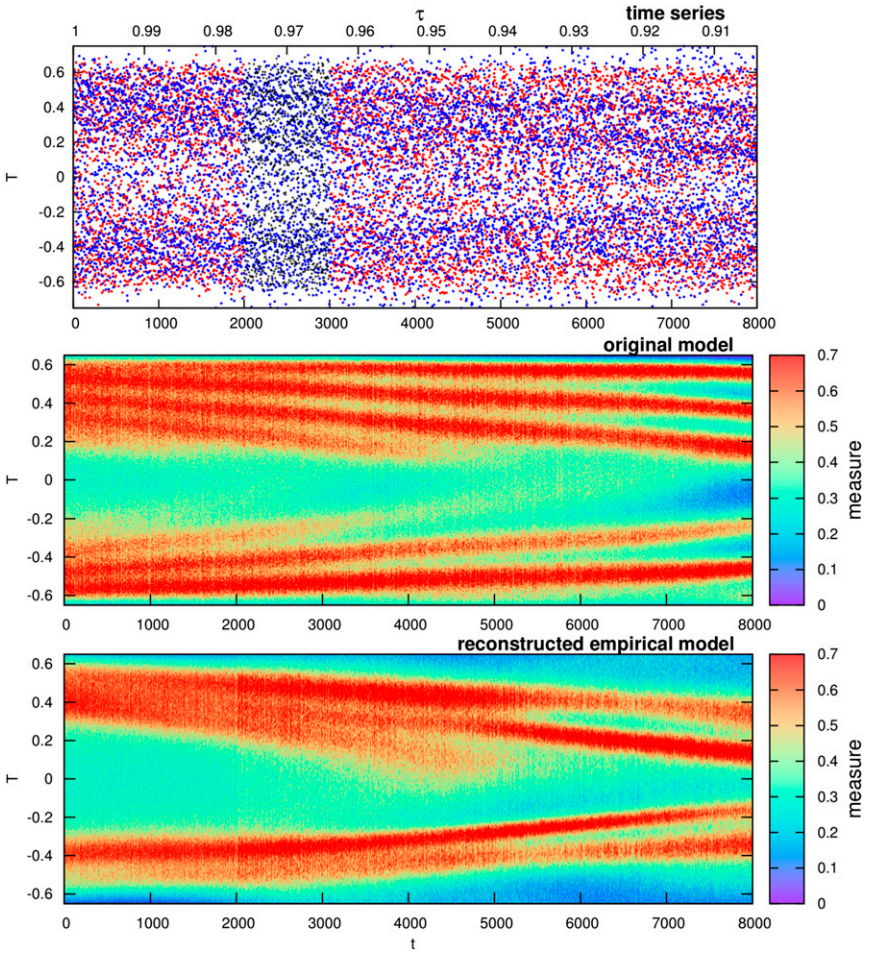

FIG. 10. As in Fig. 8, but with noise level $\sigma = 0.3$.

Fourier spectra (blue lines) with those of the original model.

c. *Galanti and Tziperman model*

As discussed in section 4b, we study this model in a parameter range in which it behaves chaotically, and we refrain from randomizing its parameters. The time series shown in the top panel of Fig. 12 was obtained as the delay τ_1 was changed linearly from 2.9 to 0.5 months over 9000 yr. The bottom panel shows the results of the reconstruction by an ANN model of dimension $d = 2$ and number of neurons $m_f = 12$ and $m_g = 2$.

The empirical model succeeds quite well in forecasting the nature of the Galanti and Tziperman (2000) model's critical transitions into both past and future, although the exact timing is somewhat off. Further confirmation of the model's skill is given by the close agreement between the dynamical and empirical models' Fourier spectra in Fig. 13. As in the Tziperman et al. (1994) model (see again Fig. 11), the QB peak is barely present here, but the evolution of the QQ peak with time in the Galanti and Tziperman (2000) model is well captured by our empirical model.

6. Concluding remarks

In this paper, we developed an approach to empirical modeling and prediction of complex dynamical systems using observed, finite intervals of the time series generated by such a system for which the evolution operator is not known. Following this approach, inverse, stochastic models were constructed to describe the key properties of the system under study and use them for the prediction of its future dynamics. The emphasis in this work is on predicting future regime changes, called here critical transitions, rather than details of a system's entire future evolution.

We applied the proposed approach to the analysis of the critical transitions characteristic of ENSO dynamics in order to understand and optimize their predictability

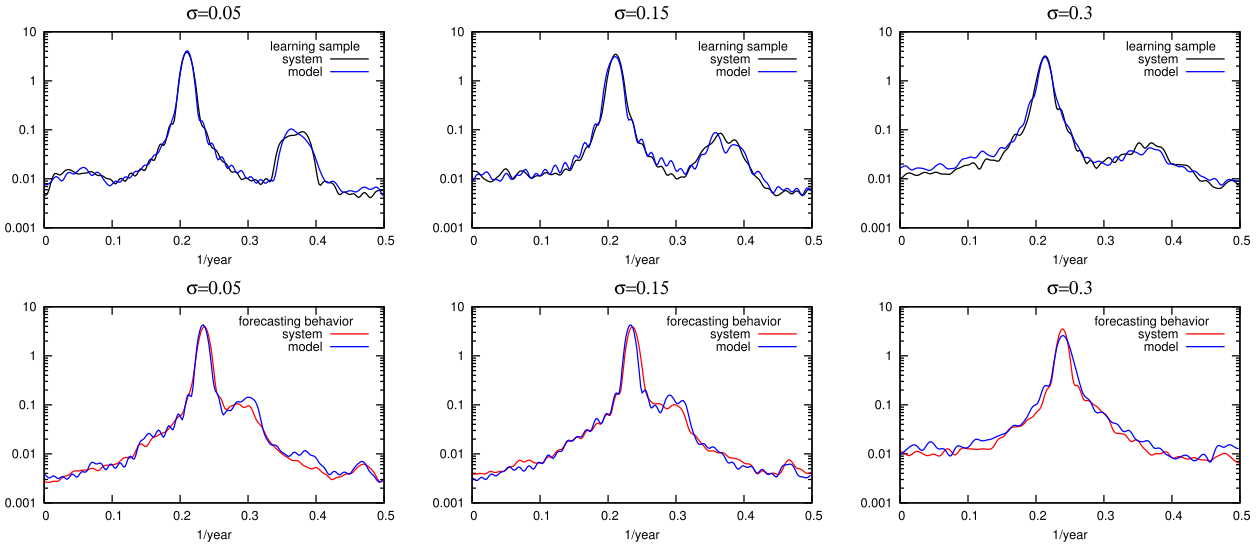

FIG. 11. As in Fig. 7, but for the Tziperman et al. (1994) model. The noise levels are σ = (left) 0.05, (center) 0.15, and (right) 0.3 (i.e., corresponding to Figs. 8–10). (top) The Fourier spectra over the training interval $2000 \le t \le 3000$; (bottom) the spectra for $4000 \le t \le 5000$.

from the observed time series. At this stage, three different, idealized models of ENSO dynamics were used to illustrate the capabilities of our approach, which will be applied to spatially distributed data in Part II. It is important to note, though, that the relatively simple models used here are of the DDE type, and, hence, are infinitely dimensional. Furthermore, they capture key elements of ENSO dynamics: namely, the seasonal forcing, nonlinear atmosphere–ocean feedbacks, and delayed adjustments due to the equatorial ocean waves.

After presenting our general approach to empirical modeling of a system's evolution operator, we provided

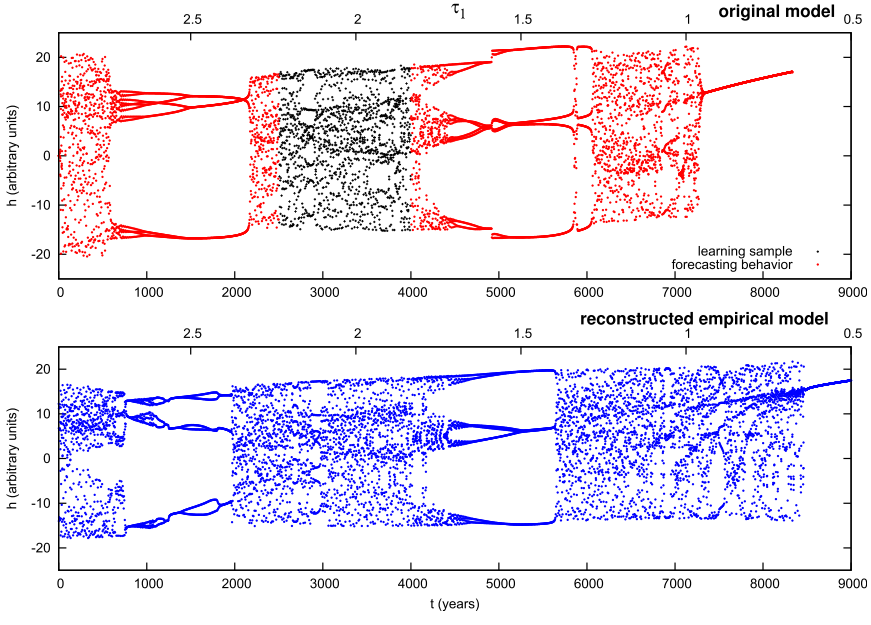

FIG. 12. Reconstruction of the Galanti and Tziperman (2000) model's behavior, governed here by Eqs. (14) and (15). The learning interval now is $2500 \le t \le 4000$ so that $N_{tr} = 1500$; the parameter τ_1 is linearly changed from 2.9 at $t = 0$ to 0.5 at $t = 9000$; and the noise level is $\sigma = 0$, while the empirical model has dimension $d = 2$, and the parameter numbers in the deterministic and stochastic parts are $m_f = 12$ and $m_g = 2$, respectively. (top) Dynamical model, with learning interval in black and the behavior outside it in red; and (bottom) empirical model in blue.

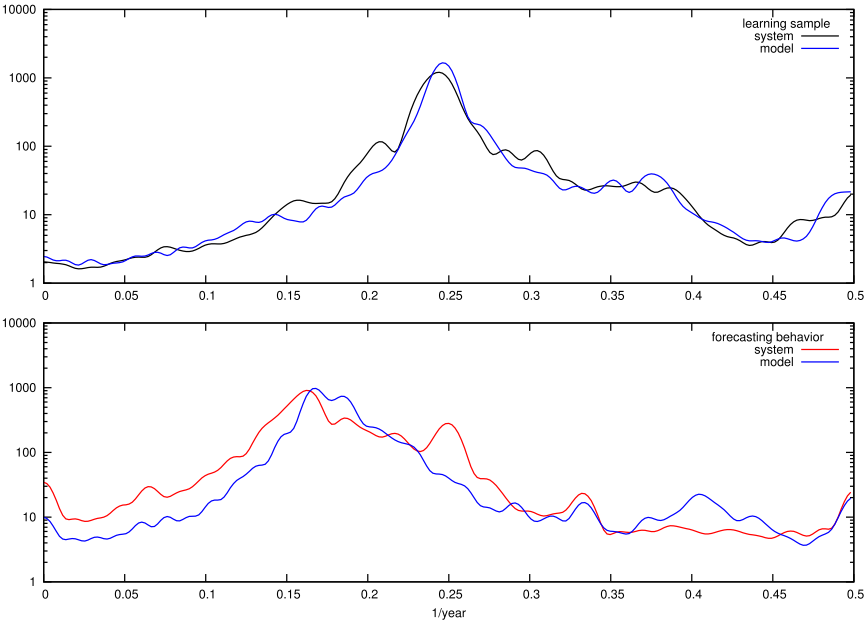

FIG. 13. Fourier spectra for the Galanti and Tziperman (2000) model. (top) Fourier spectra for the original (black) and empirical (blue) model during the learning interval $2500 \leq t \leq 4000$; (bottom) the spectra of the future behavior of the original (red) and empirical (blue) model for $6000 \leq t \leq 7000$.

an algorithm for constructing a low-dimensional approximation of this operator via artificial neural networks (ANNs). It was pointed out that the use of random processes in the algorithm is of the essence in order to explore a broader region of the empirical model's reduced phase space than the one covered by the system's trajectories during the learning interval.

The three DDE models of ENSO dynamics to which our algorithm was applied are the Tziperman et al. (1994), Galanti and Tziperman (2000), and Ghil et al. (2008b) models. Our main result is that the empirical models constructed herein are able to forecast sequences of critical transitions—manifesting themselves as abrupt changes of the system's probability density in phase space—well into the future (i.e., at times that can exceed an integer multiple of the length of the learning interval). The forecasts were overall quite accurate as to the nature of the critical transitions and sometimes but not always so with respect to the exact timing of the transitions.

Note that the nonlinearity of the empirical models—given by their ANN-based structure—is essential for capturing the critical transitions of all three DDE models we studied: these transitions correspond to certain model bifurcations and hence are strongly nonlinear in nature. Certainly, such forecasts would be impossible with any linear approach. In particular, our empirical models were able to predict critical transitions associated with the destruction of a simple attractor that exists in a narrow region of phase space and with the system's shift to a more complex dynamic regime; see, for instance, the transitions that occur in the Ghil et al. (2008b) model (Fig. 3) at $t \simeq 3200$, in the Tziperman et al. (1994) model (Fig. 8) at $t \simeq 4000$, and in the Galanti and Tziperman (2000) model (Fig. 12) at $t \simeq 700$ and 6000.

As previously stated, this study is restricted to the analysis of scalar time series generated by the conceptual models of Eqs. (12)–(14) that, while infinitely dimensional, include only one or two dynamical variables. Of course, the real atmosphere–ocean system responsible for the climate dynamics in the equatorial Pacific is much more complex than these models. However, the motivating hypothesis of empirical modeling in general is that there exist low-dimensional models that manage to approximate the current and future evolution of a high-dimensional system (Penland 1996; Kondrashov et al. 2005; Kravtsov et al. 2005, 2009). Chekroun et al. (2014) have recently shown that, under suitable mathematical conditions, this hypothesis can be shown to hold rigorously. Here, we extend this hypothesis to the very interesting case of successfully predicting critical transitions and demonstrate its validity, at first, on simple conceptual models.

The success of the present approach depends on the extent to which the learning interval contains sufficient

information on the system's behavior in the future as well. For the Galanti and Tziperman (2000) model (Figs. 12 and 13), this was the case even without the need of adding stochastic terms to the parametrically driven model; for the other two—the Ghil et al. (2008b) model (Figs. 3–7) and the Tziperman et al. (1994) model (Figs. 8–11)—it was necessary to extend the phase-space region explored during learning by such stochastic perturbations.

The main additional difficulty of working with the real climate system lies in the need to analyze much richer datasets that include multiple time series of distinct climate variables on a given spatial grid. Clearly, in that case the problem of constructing low-dimensional empirical models is more complicated than the one treated in this paper. Several studies have already shown that successful simulation and prediction of large climatic datasets using low-order inverse models is possible (Penland 1996; Penland and Matrosova 2001; Kondrashov et al. 2005; Kravtsov et al. 2009; Chekroun et al. 2011a). Part II of this paper will consider a time series generated by a spatially distributed dynamic model that describes ENSO dynamics and will suggest a way to construct a low-order empirical model that is able to effectively forecast critical transitions using the observed time series measured at distributed spatial locations.

Acknowledgments. It is a pleasure to thank Mickael D. Chekroun for providing the data from his calculations that used the Galanti and Tziperman (2000) model and for participating in the discussions that led to this paper. Dmitri Kondrashov has greatly helped with improving the figures. Three reviewers provided very insightful and constructive suggestions to this two-part paper. Our work benefited from the support of the CRDF Global–Russian Foundation for Basic Research (RFBR) program in Multidisciplinary Climate Change (Project RUG1-2977-NN-10) and the Government of the Russian Federation (Agreement No. 14.Z50.31.0033). Additional support was provided by Grants DMS-0934426 and DMS-1049092 (MDC, MG, and IZ) and OCE-1243175 (MDC, MG, and DK) from the U.S. National Science Foundation, and by MURI Grant N00014-12-1-0911 from the U.S. Office of Naval Research (MDC, MG, and DK).

REFERENCES

Abraham, R., and J. E. Marsden, 1987: *Foundations of Mechanics.* 2nd ed. Addison-Wesley, 826 pp.

Arnold, L., 1998: *Random Dynamical Systems.* Springer Monographs in Mathematics, Springer-Verlag, 581 pp.

Barnston, A. G., M. K. Tippett, M. L. L'Heureux, S. Li, and D. G. DeWitt, 2012: Skill of real-time seasonal ENSO model predictions during 2002–2011: Is our capability increasing? *Bull. Amer. Meteor. Soc.,* **93,** 631–651, doi:10.1175/BAMS-D-11-00111.1.

Battisti, D. S., 1988: Dynamics and thermodynamics of a warming event in a coupled tropical atmosphere–ocean model. *J. Atmos. Sci.,* **45,** 2889–2919, doi:10.1175/1520-0469(1988)045<2889:DATOAW>2.0.CO;2.

——, and A. C. Hirst, 1989: Interannual variability in a tropical atmosphere–ocean model: Influence of the basic state, ocean geometry and nonlinearity. *J. Atmos. Sci.,* **46,** 1687–1712, doi:10.1175/1520-0469(1989)046<1687:IVIATA>2.0.CO;2.

Bhattacharya, K., M. Ghil, and I. Vulis, 1982: Internal variability of an energy-balance model with delayed albedo effects. *J. Atmos. Sci.,* **39,** 1747–1773, doi:10.1175/1520-0469(1982)039<1747:IVOAEB>2.0.CO;2.

Bjerknes, J., 1969: Atmospheric teleconnections from the equatorial Pacific. *Mon. Wea. Rev.,* **97,** 163–172, doi:10.1175/1520-0493(1969)097<0163:ATFTEP>2.3.CO;2.

Chang, P., B. Wang, T. Li, and L. Ji, 1994: Interactions between the seasonal cycle and the Southern Oscillation—Frequency entrainment and chaos in a coupled ocean–atmosphere model. *Geophys. Res. Lett.,* **21,** 2817–2820, doi:10.1029/94GL02759.

——, L. Ji, B. Wang, and T. Li, 1995: Interactions between the seasonal cycle and El Niño–Southern Oscillation in an intermediate coupled ocean–atmosphere model. *J. Atmos. Sci.,* **52,** 2353–2372, doi:10.1175/1520-0469(1995)052<2353:IBTSCA>2.0.CO;2.

Chao, Y., M. Ghil, and J. C. McWilliams, 2000: Pacific interdecadal variability in this century's sea surface temperatures. *Geophys. Res. Lett.,* **27,** 2261–2264, doi:10.1029/1999GL011324.

Chekroun, M. D., D. Kondrashov, and M. Ghil, 2011a: Predicting stochastic systems by noise sampling, and application to the El Niño–Southern Oscillation. *Proc. Natl. Acad. Sci. USA,* **108,** 11 766–11 771, doi:10.1073/pnas.1015753108.

——, E. Simonnet, and M. Ghil, 2011b: Stochastic climate dynamics: Random attractors and time-dependent invariant measures. *Physica D,* **240,** 1685–1700, doi:10.1016/j.physd.2011.06.005.

——, J. D. Neelin, D. Kondrashov, J. C. McWilliams, and M. Ghil, 2014: Rough parameter dependence in climate models and the role of Ruelle–Pollicott resonances. *Proc. Natl. Acad. Sci. USA,* **111,** 1684–1690, doi:10.1073/pnas.1321816111.

Diaz, H. F., and V. Markgraf, Eds., 1992: *El Niño.* Cambridge University Press, 492 pp.

Dijkstra, H. A., and M. Ghil, 2005: Low-frequency variability of the large-scale ocean circulation: A dynamical systems approach. *Rev. Geophys.,* **43,** RG3002, doi:10.1029/2002RG000122.

Eckmann, J.-P., and D. Ruelle, 1985: Ergodic theory of chaos and strange attractors. *Rev. Mod. Phys.,* **57,** 617–656, doi:10.1103/RevModPhys.57.617.

Galanti, E., and E. Tziperman, 2000: ENSO's phase locking to the seasonal cycle in the fast-SST, fast-wave, and mixed-mode regimes. *J. Atmos. Sci.,* **57,** 2936–2950, doi:10.1175/1520-0469(2000)057<2936:ESPLTT>2.0.CO;2.

Ghil, M., 1994: Cryothermodynamics: The chaotic dynamics of paleoclimate. *Physica D,* **77,** 130–159, doi:10.1016/0167-2789(94)90131-7.

——, 2001: Hilbert problems for the geosciences in the 21st century. *Nonlin. Processes Geophys.,* **8,** 211–222, doi:10.5194/npg-8-211-2001.

——, 2015: A mathematical theory of climate sensitivity or, how to deal with both anthropogenic forcing and natural variability? *Climate Change: Multidecadal and Beyond,* C.-P. Chang, et al., Eds., World Scientific Series on Asia-Pacific Weather and Climate, Vol. 6, World Scientific, in press.

——, and S. Childress, 1987: *Topics in Geophysical Fluid Dynamics: Atmospheric Dynamics, Dynamo Theory, and Climate Dynamics.* Applied Mathematical Sciences, Vol. 60, Springer-Verlag, 512 pp.

——, and N. Jiang, 1998: Recent forecast skill for the El Niño/Southern Oscillation. *Geophys. Res. Lett.,* **25,** 171–174, doi:10.1029/97GL03635.

——, and A. W. Robertson, 2000: Solving problems with GCMs: General circulation models and their role in the climate modeling hierarchy. *General Circulation Model Development: Past, Present, and Future,* D. Randall, Ed., International Geophysics Series, Vol. 70, Academic Press, 285–325.

——, and I. Zaliapin, 2013: El Niño/Southern Oscillation: Impacts, modeling and forecasts. *Encyclopedia of Natural Hazards,* P. Bobrowsky, Ed., Springer, 250–262.

——, and Coauthors, 2002: Advanced spectral methods for climatic time series. *Rev. Geophys.,* **40,** 1003, doi:10.1029/2000rg000092.

——, M. D. Chekroun, and E. Simonnet, 2008a: Climate dynamics and fluid mechanics: Natural variability and related uncertainties. *Physica D,* **237,** 2111–2126, doi:10.1016/j.physd.2008.03.036.

——, I. Zaliapin, and S. Thompson, 2008b: A delay differential model of ENSO variability: Parametric instability and the distribution of extremes. *Nonlin. Processes Geophys.,* **15,** 417–433, doi:10.5194/npg-15-417-2008.

Hale, J. K., and S. M. V. Lunel, 1993: *Introduction to Functional Differential Equations.* Applied Mathematical Sciences, Vol. 99, Springer, 450 pp.

Hornik, K., M. Stinchcombe, and H. White, 1989: Multilayer feedforward networks are universal approximators. *Neural Networks,* **2,** 359–366, doi:10.1016/0893-6080(89)90020-8.

Huybers, P., 2009: Pleistocene glacial variability as a chaotic response to obliquity forcing. *Climate Past,* **5,** 481–488, doi:10.5194/cp-5-481-2009.

Jiang, N., J. Neelin, and M. Ghil, 1995: Quasi-quadrennial and quasi-biennial variability in the equatorial Pacific. *Climate Dyn.,* **12,** 101–112, doi:10.1007/BF00223723.

Jin, F.-F., 1997a: An equatorial ocean recharge paradigm for ENSO. Part I: Conceptual model. *J. Atmos. Sci.,* **54,** 811–829, doi:10.1175/1520-0469(1997)054<0811:AEORPF>2.0.CO;2.

——, 1997b: An equatorial ocean recharge paradigm for ENSO. Part II: A stripped-down coupled model. *J. Atmos. Sci.,* **54,** 830–847, doi:10.1175/1520-0469(1997)054<0830:AEORPF>2.0.CO;2.

——, J. D. Neelin, and M. Ghil, 1994: El Niño on the devil's staircase: Annual subharmonic steps to chaos. *Science,* **264,** 70–72, doi:10.1126/science.264.5155.70.

——, ——, and ——, 1996: El Niño/Southern Oscillation and the annual cycle: Subharmonic frequency-locking and aperiodicity. *Physica D,* **98,** 442–465, doi:10.1016/0167-2789(96)00111-X.

Kadanoff, L. P., 1983: Roads to chaos. *Phys. Today,* **36,** 4653, doi:10.1063/1.2915388.

Kondrashov, D., S. Kravtsov, A. W. Robertson, and M. Ghil, 2005: A hierarchy of data-based ENSO models. *J. Climate,* **18,** 4425–4444, doi:10.1175/JCLI3567.1.

Kravtsov, S., D. Kondrashov, and M. Ghil, 2005: Multilevel regression modeling of nonlinear processes: Derivation and applications to climatic variability. *J. Climate,* **18,** 4404–4424, doi:10.1175/JCLI3544.1.

——, ——, and ——, 2009: Empirical model reduction and the modelling hierarchy in climate dynamics and the geosciences. *Stochastic Physics and Climate Modelling,* T. N. Palmer and P. Williams, Eds., Cambridge University Press, 35–72.

Latif, M., T. Barnett, M. Cane, M. Flügel, N. Graham, H. von Storch, J.-S. Xu, and S. Zebiak, 1994: A review of ENSO prediction studies. *Climate Dyn.,* **9,** 167–179, doi:10.1007/BF00208250.

Madden, R. A., and P. R. Julian, 1994: Observations of the 40–50-day tropical oscillation—A review. *Mon. Wea. Rev.,* **122,** 814–837, doi:10.1175/1520-0493(1994)122<0814:OOTDTO>2.0.CO;2.

Mañe, R., 1981: On the dimension of the compact invariant sets of certain non-linear maps. *Dynamical Systems and Turbulence,* D. A. Rand and L.-S. Young, Eds., Lecture Notes in Mathematics, Vol. 898, Springer-Verlag, 230–242.

Molkov, Y. I., D. N. Mukhin, E. M. Loskutov, R. I. Timushev, and A. M. Feigin, 2011: Prognosis of qualitative system behavior by noisy, nonstationary, chaotic time series. *Phys. Rev.,* **84E,** 036215, doi:10.1103/PhysRevE.84.036215.

——, E. M. Loskutov, D. N. Mukhin, and A. M. Feigin, 2012: Random dynamical models from time series. *Phys. Rev.,* **85E,** 036216, doi:10.1103/PhysRevE.85.036216.

Mukhin, D., D. Kondrashov, E. Loskutov, A. Gavrilov, A. Feigin, and M. Ghil, 2015: Predicting critical transitions in ENSO models. Part II: Spatially dependent models. *J. Climate,* **28,** 1962–1976, doi:10.1175/JCLI-D-14-00240.1.

Münnich, M., M. A. Cane, and S. E. Zebiak, 1991: A study of self-excited oscillations of the tropical ocean–atmosphere system. Part II: Nonlinear cases. *J. Atmos. Sci.,* **48,** 1238–1248, doi:10.1175/1520-0469(1991)048<1238:ASOSEO>2.0.CO;2.

Neal, R. M., 1993: Probabilistic inference using Markov chain Monte Carlo methods. Department of Computer Science, University of Toronto Tech. Rep. CRG-TR-93-1, 140 pp.

Penland, C., 1996: A stochastic model of IndoPacific sea surface temperature anomalies. *Physica D,* **98,** 534–558, doi:10.1016/0167-2789(96)00124-8.

——, and L. Matrosova, 2001: Expected and actual errors of linear inverse model forecasts. *Mon. Wea. Rev.,* **129,** 1740–1745, doi:10.1175/1520-0493(2001)129<1740:EAAEOL>2.0.CO;2.

Philander, S. G., 1990: *El Niño, La Niña, and the Southern Oscillation.* Academic Press, 293 pp.

Press, W. H., S. A. Teukolsky, W. T. Vetterling, and B. P. Flannery, 2002: *Numerical Recipes in C++: The Art of Scientific Computing.* 2nd ed. Cambridge University Press, 1002 pp.

Runborg, O., C. Theodoropoulos, and I. G. Kevrekidis, 2002: Effective bifurcation analysis: A time-stepper-based approach. *Nonlinearity,* **15,** 491, doi:10.1088/0951-7715/15/2/314.

Scheffer, M., 2009: *Critical Transitions in Nature and Society.* Princeton University Press, 400 pp.

Suarez, M. J., and P. S. Schopf, 1988: A delayed action oscillator for ENSO. *J. Atmos. Sci.,* **45,** 3283–3287, doi:10.1175/1520-0469(1988)045<3283:ADAOFE>2.0.CO;2.

Takens, F., 1981: Detecting strange attractors in turbulence. *Dynamical Systems and Turbulence,* D. A. Rand and L.-S. Young, Eds., Lecture Notes in Mathematics, Vol. 898, Springer-Verlag, 366–381.

Theodoropoulos, C., Y.-H. Qian, and I. G. Kevrekidis, 2000: "Coarse" stability and bifurcation analysis using time-steppers: A reaction-diffusion example. *Proc. Natl. Acad. Sci. USA,* **97,** 9840–9843, doi:10.1073/pnas.97.18.9840.

Timmermann, A., and F.-F. Jin, 2006: Predictability of coupled processes. *Predictability of Weather and Climate,* T. Palmer and R. Hagedorn, Eds., Cambridge University Press, 251–274.

Trenberth, K., and J. W. Hurrell, 1994: Decadal atmosphere–ocean variations in the Pacific. *Climate Dyn.,* **9,** 303–319, doi:10.1007/BF00204745.

Tziperman, E., L. Stone, M. A. Cane, and H. Jarosh, 1994: El Niño chaos: Overlapping of resonances between the seasonal cycle and the Pacific ocean–atmosphere oscillator. *Science,* **264,** 72–74, doi:10.1126/science.264.5155.72.

——, M. A. Cane, and S. E. Zebiak, 1995: Irregularity and locking to the seasonal cycle in an ENSO prediction model as explained by the quasi-periodicity route to chaos. *J. Atmos. Sci.,* **52,** 293–306, doi:10.1175/1520-0469(1995)052<0293:IALTTS>2.0.CO;2.

Zaliapin, I., and M. Ghil, 2010: Another look at climate sensitivity. *Nonlin. Processes Geophys.,* **17,** 113–122, doi:10.5194/npg-17-113-2010.

Zebiak, S. E., and M. A. Cane, 1987: A model El Niño–Southern Oscillation. *Mon. Wea. Rev.,* **115,** 2262–2278, doi:10.1175/1520-0493(1987)115<2262:AMENO>2.0.CO;2.